Neurobiology of Disease

Protein Kinase C Lambda Mediates Acid-Sensing Ion Channel 1a-Dependent Cortical Synaptic Plasticity and Pain Hypersensitivity

Hu-Song Li,[1]* Xin-Yu Su,[1]* Xing-Lei Song,[1] Xin Qi,[1] Ying Li,[1] Rui-Qi Wang,[1] Oleksandr Maximyuk,[2] Oleg Krishtal,[2] Tingting Wang,[3] Houqin Fang,[3] Lujian Liao,[3] Hong Cao,[4] Yu-Qiu Zhang,[4], Michael X. Zhu,[5] Ming-Gang Liu,[1] and Tian-Le Xu[1]

[1]Collaborative Innovation Center for Brain Science, Department of Anatomy and Physiology, Shanghai Jiao Tong University School of Medicine, Shanghai 200025, China, [2]Bogomoletz Institute of Physiology of NAS Ukraine, 01024 Kyiv, Ukraine, [3]Shanghai Key Laboratory of Regulatory Biology, and Shanghai Key Laboratory of Brain Functional Genomics, School of Life Sciences, East China Normal University, Shanghai 200241, China, [4]State Key Laboratory of Medical Neurobiology and MOE Frontiers Center for Brain Science, Institute of Brain Science, Fudan University, Shanghai 200032, China, and [5]Department of Integrative Biology and Pharmacology, McGovern Medical School, University of Texas Health Science Center at Houston, Houston, Texas 77030

Chronic pain is a serious debilitating disease for which effective treatment is still lacking. Acid-sensing ion channel 1a (ASIC1a) has been implicated in nociceptive processing at both peripheral and spinal neurons. However, whether ASIC1a also contributes to pain perception at the supraspinal level remains elusive. Here, we report that ASIC1a in ACC is required for thermal and mechanical hypersensitivity associated with chronic pain. ACC-specific genetic deletion or pharmacological blockade of ASIC1a reduced the probability of cortical LTP induction and attenuated inflammatory thermal hyperalgesia and mechanical allodynia in male mice. Using cell type-specific manipulations, we demonstrate that ASIC1a in excitatory neurons of ACC is a major player in cortical LTP and pain behavior. Mechanistically, we show that ASIC1a tuned pain-related cortical plasticity through protein kinase C λ-mediated increase of membrane trafficking of AMPAR subunit GluA1 in ACC. Importantly, postapplication of ASIC1a inhibitors in ACC reversed previously established nociceptive hypersensitivity in both chronic inflammatory pain and neuropathic pain models. These results suggest that ASIC1a critically contributes to a higher level of pain processing through synaptic potentiation in ACC, which may serve as a promising analgesic target for treatment of chronic pain.

Key words: acid-sensing ion channel; ACC; chronic pain; long-term potentiation; protein kinase C

Significance Statement

Chronic pain is a debilitating disease that still lacks effective therapy. Ion channels are good candidates for developing new analgesics. Here, we provide several lines of evidence to support an important role of cortically located ASIC1a channel in pain hypersensitivity through promoting long-term synaptic potentiation in the ACC. Our results indicate a promising translational potential of targeting ASIC1a to treat chronic pain.

Introduction

Chronic pain is a challenging clinical problem seriously affecting millions of people everyday (Holmes, 2016). Unfortunately, the current treatment for chronic pain is not very effective (Woolf, 2010; Yekkirala et al., 2017). The most widely used analgesics for chronic pain are opioids and aspirin-like nonsteroidal anti-

Received Jan. 24, 2019; revised May 12, 2019; accepted May 14, 2019.

Author contributions: H.-S.L., X.-Y.S., X.-L.S., X.Q., Y.L., and R.-Q.W. performed research; H.-S.L. and M.-G.L. analyzed data; H.-S.L. wrote the first draft of the paper; O.M., O.K., T.W., H.F., L.L., H.C., and Y.-Q.Z. contributed unpublished reagents/analytic tools; M.X.Z. edited the paper; M.X.Z., M.-G.L., and T.-L.X. wrote the paper; M.-G.L. and T.-L.X. designed research.

This work was supported by National Natural Science Foundation of China Grants 81730095, 31771157, and 91632304; Science and Technology Commission of Shanghai Municipality 18JC1420302; Shanghai Municipal Science and Technology Major Project 2018SHZDZX05; and Shanghai Jiao Tong University School of Medicine Doctoral Innovation Fellowship BXJ201901. We thank Dr. John A. Wemmie, Dr. Michael J. Welsh, and Dr. Cheng-Chang Lien for kindly providing the ASIC1a KO and ASIC1a $^{flox/flox}$ used in the current study; Dr. Alexander M. Binshtok, Dr. Yuan-Xiang Tao, Dr. Hui Lu, and Dr. Wei Lu for valuable comments on earlier versions of the manuscript; and Shaoli Wang, Fan Zhao, Dr. Yang Tian, and Dr. Ning Song for technical assistance.

The authors declare no competing financial interests.

*H.-S.L. and X.-Y.S. contributed equally to this work.

Correspondence should be addressed to Ming-Gang Liu at lmg11302000@126.com or Tian-Le Xu at xu-happiness@shsmu.edu.cn.

https://doi.org/10.1523/JNEUROSCI.0213-19.2019

inflammatory drugs, for which the clinical efficacy is limited by severe adverse effects and abuse liability (Roques et al., 2012; Latremoliere and Costigan, 2018). On the other hand, pain perception eventually resides in the brain (Chen, 2018). ACC is an important forebrain structure involved in a variety of physiological and pathological functions, including chronic pain (Chen et al., 2018; Sellmeijer et al., 2018). Synaptic plasticity in ACC is considered one of the most critical mechanisms underlying the transition of pain from acute to chronic (Luo et al., 2014; Bliss et al., 2016). Peripheral inflammatory or neuropathic pain elicits dramatic plastic changes in synaptic transmission and morphology of ACC neurons (Zhao et al., 2006; Ko et al., 2018), whereas blocking or erasing aberrant cingulate plasticity produces significant analgesic effects in animals (Li et al., 2010; Wang et al., 2011).

Accordingly, molecules involved in the induction and expression of plastic changes in ACC are potential drug targets for treating chronic pain (Bliss et al., 2016). Among several candidates, NMDAR, a major glutamate receptor important for cortical LTP (Paoletti et al., 2013), has been intensively investigated as an analgesic target by academic laboratories and pharmaceutical companies. However, the use of a general NMDAR antagonist is limited by side effects, such as ataxia and sedation (Chizh et al., 2001; Wu and Zhuo, 2009). Another important glutamate receptor, AMPAR, contributes to the expression of LTP through regulated trafficking into and out of synapses (Huganir and Nicoll, 2013). However, perampanel, a noncompetitive AMPAR antagonist used to treat partial seizures for people older than 12 years, can induce serious adverse psychiatric and behavioral reactions (Ettinger et al., 2015). Because of the limitations in targeting classical glutamate receptors, it is necessary and important to explore other molecule targets for chronic pain treatment.

Ion channels are emerging as promising targets for devising and developing novel analgesics with promising therapeutic outcomes (Waxman and Zamponi, 2014; Zamponi, 2016). Acid-sensing ion channel (ASIC) family consists of six isoforms (ASIC1a, 1b, 2a, 2b, 3 and 4) encoded by four genes (Kellenberger and Schild, 2015), among which ASIC1a has been most frequently studied because of its ubiquitous expression in the brain (Wemmie et al., 2003). Previous work has unequivocally demonstrated that ASIC1a plays crucial roles in modulating pain sensitivity (Wemmie et al., 2013; Deval and Lingueglia, 2015). Peripheral administration of a Texas coral snake toxin elicits strong pain in mice through activation of ASIC1-expressing nociceptors (Bohlen et al., 2011). In contrast, intrathecal injection of mambalgin-1, a toxin isolated from black mamba venom, or psalmotoxin 1 (PcTx1), a peptide extracted from South American tarantula, produces potent analgesic effect in an ASIC1a-dependent manner (Mazzuca et al., 2007; Diochot et al., 2012). However, despite these exciting results, fewer reports have illustrated the role of supraspinally localized ASIC1a in chronic pain.

Here, we investigated the role of ASIC1a in ACC neurons in chronic pain and cortical plasticity. We found that genetic deletion or pharmacological blockade of the ASIC1a channel in ACC substantially attenuated thermal and mechanical hypersensitivities in inflammatory pain. Moreover, ASIC1a modulates pain sensitivity by promoting AMPAR GluA1 subunit trafficking and induction of LTP in ACC through protein kinase C λ (PKCλ). Importantly, post-treatments with ASIC1a inhibitors can reverse preestablished pain hypersensitivity in both inflammatory and neuropathic pain models, demonstrating a promising translational potential of targeting ASIC1a-mediated aberrant cortical plasticity to treat chronic pain.

Materials and Methods

Animals. The experiments were performed on C57BL/6J, ASIC1a WT/KO, and ASIC1a$^{flox/flox}$ mice (male, 8–10 weeks old). The global ASIC1a KO mice (RRID:MGI:2654038) were the generous gifts of Prof. Michael J. Welsh (Howard Hughes Medical Institute, University of Iowa, Iowa City, IA) (Wemmie et al., 2002). The conditional ASIC1a$^{flox/flox}$ mice (RRID:IMSR_RMRC13158) were graciously provided by Prof. Cheng-Chang Lien (National Yang-Ming University, Taiwan) (Wu et al., 2013). All mice were housed in groups of 4 or 5 per cage under standard environment (12 h light/dark cycles at 21°C and 50%–60% humidity) with mouse chow and water *ad libitum*. Animal care and the experimental procedures were approved by the Animal Ethics Committee of Shanghai Jiao Tong University School of Medicine, Shanghai, China (Policy Number DLAS-MP-ANIM.01-05).

Animal model of pain. To induce inflammatory pain, complete Freund's adjuvant (CFA, 50% in saline, 20 μl; Sigma-Aldrich) was injected into the plantar surface of the left hindpaw (Berta et al., 2014). Sham control animals received 20 μl of saline. Unless otherwise stated, pain-related behavioral tests were performed at day 1, 3, 5, and 7 after the CFA injection. For neuropathic pain, we adopted a well-established spared nerve injury (SNI) model as previously described (Bourquin et al., 2006; Chen et al., 2015; Tan et al., 2017). Briefly, the mice were anesthetized with isoflurane, and an incision was made to the lateral skin surface of the thigh to expose the sciatic nerve and its branches. Then a 5.0 silk tight ligation of the tibial and common peroneal nerves was performed, followed by transection and removal of a 3 to 5 mm portion of the nerve. However, the third peripheral branch of the sciatic nerve, the sural nerve, was left intact, and any contact with or stretching of this nerve was carefully avoided. The muscle and skin were subsequently sutured, and animals were left to recover in a heated cage for 24 h. For the sham group, the surgical procedures were almost the same, except that the nerves were only exposed but not ligated/cut. Behavioral testing was performed at 7 and 14 d after the operation.

Cannula implantation and drug microinjection. Cannulation and microinjection were performed as described previously (Wang et al., 2011; Ko et al., 2018). Animals were anesthetized and placed in a stereotaxic frame (RWD Life Science). Guide cannulas were implanted bilaterally into ACC with the following coordinates: AP 1.00 mm, lateral ±1.47 mm with a 30° angle, DV −1.65 mm from the skull. The cannulas were fixed in the position with acrylic dental cement and secured with skull screws. To prevent clogging, a stylus was placed in the guide cannula. Animals were allowed to recover from surgery for at least 1 week before experimental manipulations. For drug microinfusion, the stylus was removed from the guide cannula, and a 30-gauge injector (1.00 mm lower than the guide) cannula was used. The infusion cannula was conducted via PE20 tubing to a motorized microsyringe infusion pump (KDS 310, KD Scientific). PcTx1 (10 μM in saline, 0.5 μl per side, Peptide Institute), compound 5b (100 μM in saline, 0.5 μl per side), and their respective vehicles were microinfused into ACC at a rate of 0.1 μl/min. These drug doses were chosen based on the previous literature using the similar pharmacological strategy to study the function of ASIC1a (Buta et al., 2015; Li et al., 2016; Wang et al., 2018), as well as our preliminary experiments and calculations on the diffusion range of the drug in the ACC according to the estimated average volume of this brain region in an adult mouse. Also, we did not observe any obvious neurological deficits in the drug-infused animals, indicating the lack of significant side effects at the selected doses. After the microfusion, the injector was left in place for 10 min for the drug to diffuse and act on its targets before experimental testing. The injection sites were mapped postmortem by sectioning the brain and performing Nissl staining. Animals with incorrect diffusion scope were excluded from the data analysis.

Virus constructs. Adeno-associated virus (AAV) vectors (pAAV-MCS) carrying the full-length of WT mouse ASIC1a (NM_009597.2) or PKCλ (NM_008857.3) cDNA were constructed with the coding sequences of EYFP and mCherry fused to that of the N termini of ASIC1a and PKCλ, respectively, via the coding sequence for the "self-cleaving" 2A-peptide. To ensure specific expression of ASIC1a (or PKCλ) in neurons, human synapsin I (hSyn) promoter was used. The construct was then packaged

into AAV2/8 chimeric virus with AAV8 capsids and AAV2 ITR (inverted terminal repeat) element. The pAAV-EGFP (or pAAV-mCherry) vector driven by the hSyn promoter without ASIC1a (or PKCλ) was used as a control AAV vector (AAV-hSyn-Ctrl). The AAV vector for expression of Cre recombinase or EGFP driven by the hSyn promoter was constructed using similar methods.

To make the short hairpin RNA (shRNA) constructs, oligonucleotides that contain 21 base sense and antisense sequences targeting mouse ASIC1a (NM_009597.2, sense sequence, 5′-GGACATTCAGCAAGATGAATA-3′) were connected with a hairpin loop followed by a poly(T) termination signal (Li et al., 2016). These sequences were then cloned into the vector pGLV1-U6-GFP (Genepharm). The negative control sequence was 5′-GTTCTCCGAACGTGTCACGT-3′. The shRNA vector targeting mouse PKCλ, 5′-CTGGATTTGCTGACATCCAAG-3′ (Wang et al., 2016), was prepared by inserting oligonucleotides containing these sequences in pAAV-U6-MCS-EF1α-EGFP. Each plasmid was then packaged into rAAV2/8 particles (AAV2 ITRs; AAV8 capsid). These procedures were performed by Sunbio Medical Biotechnology. To knock out ASIC1a specifically in excitatory neurons in ASIC1a$^{flox/flox}$ mice, AAV vector for expression of Cre recombinase driven by CaMKII promoter was constructed. AAV vector for expression of EGFP driven by CaMKII promoter was used as a control in the same set of experiments.

Viral injection. For viral injection, mice at the age of 4–6 weeks were anesthetized and placed in a stereotaxic apparatus (RWD Life Science). The coordinates of ACC according to the mouse brain atlas were as follows: AP 1.00 mm, lateral ±0.30 mm, DV −1.80 mm. Viruses (titers of all vectors >1.0×10^{12} viral genome-containing particles per milliliter) were injected bilaterally (0.5 μl/side) into ACC using glass micropipettes connected with a microinfusion pump (KDS 310, KD Scientific) at a rate of 0.1 μl/min. After the microfusion, the microelectrode was left in place for an additional 10 min to allow the viruses to diffuse. Mice were allowed to recover for at least 4 weeks before behavioral or electrophysiological experiments. Targeting was confirmed postmortem with fluorescence above background in ACC bilaterally.

Open field test. After intra-ACC administration of saline or PcTx1 as described above, each mouse was placed in the center of a square Plexiglas open field apparatus (40 × 40 × 35 cm) and allowed to freely explore for 30 min. Activity was recorded and analyzed using the Ethovision video-tracking system (Noldus Information Technology). Time spent and distances traveled in the center zone (covering 20 cm × 20 cm) were used as the measure of anxiety. Total distance traveled in the open field was also measured and analyzed to assess the motor ability of the animal.

Hargreaves' test. Thermal hyperalgesia was assessed by measuring paw withdrawal latencies in response to a radiant heat source using Hargreaves' test. Briefly, mice were placed in a transparent plastic box (10 × 10 × 5 cm) on an elevated glass plate. Thermal stimulation was delivered to the hindpaw from an infrared source (Ugo Basile) placed under the glass plate. Paw withdrawal latency was recorded by the length of time between the start of the infrared light and the foot withdrawal. Paw withdrawal latencies were averaged from at least three consecutive tests, with a minimum of 10 min between individual measurements.

von Frey test. Mechanical allodynia was examined by measuring paw withdrawal thresholds in response to mechanical stimuli (calibrated von Frey filaments). Briefly, the animal was placed in a transparent plastic box (10 × 10 × 5 cm) on an elevated mesh screen. Calibrated von Frey filaments with ascending order (0.07, 0.16, 0.40, 0.60, 1.00, 1.40, and 2.00 g) were used to stimulate the plantar surface of mouse hindpaw. Paw withdrawal threshold was determined by a modified up-down method as previously described (Chaplan et al., 1994).

Place escape/avoidance paradigm (PEAP). PEAP testing was conducted as described previously (LaBuda and Fuchs, 2000; LaGraize et al., 2004; Han et al., 2014). Individual mice were placed in a 50 × 30 × 30 cm chamber on top of a raised mesh floor with one-half painted white (light area) and the other half painted black (dark area). Animals were allowed unrestricted movement throughout the test chamber. A suprathreshold mechanical stimulus (4.0 g, von Frey filament) was applied to the plantar surface of the hindpaws at 15 s intervals throughout the 30 min test period. The mechanical stimulus was applied to the affected paw (ipsilateral to the CFA/SNI) while the animal was located in the dark area, and the naive paw (contralateral to the CFA/SNI) was stimulated when the animal was in the light area. Saline-injected and sham-ligated animals were mechanically stimulated in an identical manner as the experimental group. The percentage of time spent on the nonpreferred light side was used to quantify the level of pain affect according to previous methods (LaBuda and Fuchs, 2000; Han et al., 2014).

Subcellular fractionation. The ACC membrane fractions were prepared 3 d after CFA treatment as described previously (Xu et al., 2008; Duan et al., 2012). Briefly, ACC samples were homogenized in a lysis buffer (10 mM Tris, pH 7.4, 300 mM sucrose, and 1 mM EDTA) containing protease inhibitor mixture and then centrifuged at 8000 × g for 5 min at 4°C. The pellet (P1) containing nuclei and cell debris was discarded. The supernatant (S1) was then centrifuged at 40,000 × g for 30 min at 4°C to obtain crude membranes in pellet (P2). This pellet (P2), which included cellular membranes, was resuspended in the lysis buffer with protease inhibitor mixture. Protein contents in P2 were quantified using Pierce BCA Protein Assay Kit (Thermo Fisher Scientific). The expression of GluA1 and ASIC1a in P2 (membrane fractions) was characterized by Western blotting. Cadherin was used as the loading control of membrane extracts.

Primary culture of mouse cortical neurons. Cultured cortical neurons were prepared as described previously (Zeng et al., 2013; Wang et al., 2015). Postnatal day 1 C57BL/6 WT or ASIC1a KO mice (with a congenic C57BL/6 background) were anesthetized with halothane. Brains were removed rapidly and placed in ice-cold Ca^{2+}- and Mg^{2+}-free PBS. Tissues were dissected and incubated with 0.05% trypsin-EDTA for 15 min at 37°C, followed by trituration with fire-polished glass pipettes, and plated in poly-D-lysine-coated 35 mm culture dishes (5×10^5 cells per dish). Neurons were cultured with Neurobasal medium containing 2% B27 and 1% Glutamax supplements and maintained in a humidified 5% CO_2 atmosphere incubator. Cultures were fed twice a week and used for all the assays 14–16 d after plating. Glial growth was suppressed by the addition of 5-fluoro-2-deoxyuridine (20 μg/ml; Sigma-Aldrich) and uridine (20 μg/ml; Sigma-Aldrich). For Western blot analysis, cultured cortical neurons were treated with an acidic solution, pH 6.0, for 10 min before being homogenized for protein sample preparation. In some experiments, we applied a Ca^{2+}-free (with no Ca^{2+} added and the addition of 0.1 mM EGTA) pH 6.0 solution or a pH 6.0 solution pretreated with BAPTA-AM (30 μM) for 30 min to test the Ca^{2+} dependence of acidosis-induced PKCλ phosphorylation. The pH 7.4 extracellular solution (Ca^{2+}-free or not) was used as a control.

Neuron transfection and calcium imaging. Calcium phosphate transfection was performed in cultured cortical neurons grown on glass coverslips on 7–10 DIV. Before transfection, the culture medium was changed for fresh Neurobasal medium, and the original medium was readded. For the 35 mm dish, 1–4 μg of GCaMP6 plasmid was added into 60 μl $CaCl_2$ solution (0.3 M) with pipetting; then 60 μl HBSS (280 mM NaCl, 1.5 mM Na_2HPO_4, 50 mM HEPES, pH 6.9) was added. After fully mixing, the transfection solution was immediately transferred into the dish. After incubation at 37°C for 1–1.5 h, the medium was replaced with CO_2-saturated Neurobasal medium (wash medium) to remove excess calcium phosphate particles. After that, the wash medium was replaced with 1 ml of the original medium and 1 ml of fresh Neurobasal medium plus B27 supplement and the dish returned to the culture incubator.

At 14–16 DIV, calcium imaging experiments were performed in neurons transfected with GCaMP6. The neurons on coverslip were mounted in standard extracellular solution and consecutively imaged using a Nikon A1R laser scanning confocal microscope with a 20× lens. GCaMP6 was excited with a 488 nm laser. Baseline recording under pH 7.4 (60 s) was rapidly changed to pH 6.0 (20 s), followed by pH 7.4 perfusion for another 50 s. GCaMP6 fluorescence change ($\Delta F/F_0$) representing Ca^{2+} alterations was calculated by $(F - F_0)/F_0$, where F_0 refers to the median of the fluorescence values during the baseline period (from 0 to 60 s).

Western blotting. Protein samples from different regions of mouse brain or from cultured cortical neurons were separated in SDS-polyacrylamide gel and transferred to polyvinylidene difluoride membranes (GE Healthcare Life Science). The membranes were blocked in 5% nonfat milk for 2 h at room temperature and incubated overnight at 4°C with appropriate antibodies. Secondary antibodies conjugated to

HRP were added to the membranes and incubated for 1 h at room temperature followed by detection of the proteins with ECL solution. The visualization was performed via the ImageQuant LAS4000 Molecular Imaging System (GE Healthcare Life Sciences), and the density of immunoblots of proteins was quantified with National Institutes of Health ImageJ software (RRID:SCR_003070). Antibodies used were as follows: ASIC1a (1:500, Santa Cruz Biotechnology, sc-13905; RRID:AB_633517), GAPDH (1:1000, KangChen, KC-5G4, RRID:AB_2493106), α-tubulin (1:1000, Sigma-Aldrich, T8203, RRID:AB_1841230), GluN2B (1:1000, Millipore, MAB5220, RRID:AB_2112925), GluA1 (1:1000, Millipore, AB1504, RRID:AB_2113602), pan-Cadherin (1:1000, Abcam, ab6528, RRID:AB_305544), phosphorylated PKCλ (p-PKCλ, 1:5000, Abcam, ab5813, RRID:AB_305131), PKCλ (1:1000, Cell Signaling Technology, 2998, RRID:AB_2171737), and PKMζ (1:1000, Santa Cruz Biotechnology, sc-216, RRID:AB_2300359). The specificity of all antibodies used in this study has been validated in previous literature (Kutsuwada et al., 1996; Zamanillo et al., 1999; Volk et al., 2013; Wang et al., 2016) and separately validated again by us in our preliminary experiments using appropriate controls (data not shown).

Immunohistochemistry. After appropriate survival times, animals were anesthetized and perfused with PBS followed by 4% PFA in 0.1 M phosphate buffer, pH 7.4. The brains were postfixed at 4°C overnight, immersed in 30% sucrose for 24–48 h at 4°C for cryoprotection, and then frozen in OCT. Transverse sections (30 μm) were cut on a cryotome (Leica Microsystems). After being blocked with PBS containing 10% donkey serum and 0.5% Triton X-100 for 2 h at room temperature, the free floating ACC sections were incubated overnight at 4°C with rabbit anti-NeuN (1:500, Cell Signaling Technology, 12943, RRID:AB_2630395) or mouse anti-Vglut2 (1:500, Millipore, MAB5504, RRID:AB_2187552) in PBS with 2% normal donkey serum and 0.1% Triton X-100. After three 10 min rinses, the sections were then incubated in AlexaFluor-568-conjugated donkey anti-rabbit IgG (1:500, Invitrogen, A10042, RRID:AB_2534017) or AlexaFluor-568-conjugated donkey anti-mouse IgG (1:500, Invitrogen, A10037, RRID:AB_2534013) for 2 h at room temperature. After three 10 min rinses, the sections were incubated in DAPI (1:2000; Sigma-Aldrich, D9542) for 10 min at room temperature and then washed. The sections were finally mounted using ProLong Gold Antifade Mountant (Thermo Fisher Scientific) and then observed with a Leica Microsystems SP8 confocal laser scanning microscope.

Brain slice preparation and patch-clamp recordings. Experiments were performed on ACC slices as described previously (Koga et al., 2015; Song et al., 2017). Briefly, after decapitation, the mouse brain was quickly removed and placed in well-oxygenated (95% O_2/5% CO_2, v/v) ice-cold aCSF containing the following (in mM): 125 NaCl, 2.5 KCl, 12.5 D-glucose, 1 $MgCl_2$, 2 $CaCl_2$, 1.25 NaH_2PO_4, and 25 $NaHCO_3$, pH 7.35–7.45. Three coronal brain slices (300 μm) were obtained at the level of ACC with a vibratome (Leica Microsystems VT 1000S) and incubated at 31°C in oxygenated aCSF for at least 1 h. Then the brain slice was transferred to a recording chamber placed on the stage of a microscope (Olympus, BX51WI) equipped with an infrared differential interference contrast video monitor. EPSCs were recorded from layer II/III pyramidal neurons with an Axon 200B amplifier (Molecular Devices), and the stimulations were delivered by a bipolar tungsten stimulating electrode placed in layer V/VI of the ACC (Song et al., 2017). The recording pipettes (3–5 MΩ) were filled with a solution containing the following (in mM): 132.5 Cs-gluconate, 17.5 CsCl, 2 $MgCl_2$, 0.5 EGTA, 10 HEPES, 4 Mg-ATP, and 5 QX-314 chloride (280–300 mOsm, pH 7.2 with CsOH).

AMPAR-mediated EPSCs were induced by repetitive stimulations at 0.03 Hz, and neurons were voltage-clamped at −70 mV, except where indicated otherwise. The input-output relation of EPSCs was obtained by giving different stimulation intensities onto layer V/VI of the ACC slice. Paired-pulse facilitation was induced by delivering two consecutive pulses with a 25, 50, 75, or 100 ms interpulse interval and calculated as the ratios of the second response peak values over the first response peak values. To isolate ASIC1a-dependent synaptic currents, we treated the ACC slice from either WT or ASIC1a KO mice with CNQX (20 μM) and D-APV (50 or 100 μM) after obtaining stable AMPAR-mediated EPSCs with different stimulation intensities under the voltage-clamp mode. Then amiloride (200 μM) or PcTx1 (100 nM) was applied to ensure the involvement of ASIC1 in the relatively small remaining current after blocking AMPAR- and NMDAR-mediated synaptic transmission (Du et al., 2014; Kreple et al., 2014). To determine AMPAR/NMDAR ratio, peak amplitude of EPSCs at −70 mV in the presence of picrotoxin (100 μM) was measured as AMPAR-mediated currents, and peak amplitude of EPSCs at 40 mV in the presence of picrotoxin (100 μM) and CNQX (20 μM) was measured as NMDAR-mediated currents. The mEPSCs of superficial layer (layer II and III) pyramidal neurons in ACC were obtained at −70 mV in the presence of TTX (0.5 μM) and picrotoxin (100 μM) without stimulation and analyzed using MiniAnalysis (Synaptosoft, RRID:SCR_002184). Spiking activity of ACC neurons was measured under current-clamp mode with an internal solution containing the following (in mM): 145 K-gluconate, 5 NaCl, 10 HEPES, 2 MgATP, 0.1 Na_3GTP, 0.2 EGTA, and 1 $MgCl_2$ (280–300 mOsm, pH 7.2 with KOH). The initial access resistance was 15–30 MΩ, and it was monitored throughout the experiment. Data were discarded if the access resistance changed >20% during experiment.

Multichannel field potential recordings. A commercial 64-channel multisite recording system (MED64; Alpha-Med Sciences) was used for extracellular field potential recordings. The procedure for preparation of the MED64 probe (MED64 probe, P515A) followed standard methods as previously described (Liu et al., 2016). Slice preparation for the MED64 recording was based on the procedures mentioned above. Acutely prepared ACC slices were allowed to recover for at least 2 h at 31°C in oxygenated aCSF. Then one slice was positioned on the MED64 probe in such a way that the area of ACC was entirely covered by the recording dish mounted on the stage of an inverted microscope (IX51, Olympus). The slice was continuously perfused with oxygenated and fresh aCSF at a rate of 2 ml/min with the aid of a peristaltic pump (Minipuls 3; Gilson) throughout the experimental period.

After the slice had been allowed to recover for 20 min on the probe, one of the microelectrodes covering the deep layer V-VI of the ACC slice was selected for stimulation by visual observation through a charge-coupled device camera (DP70; Olympus) connected to the inverted microscope. For test stimulation, monopolar, biphasic constant-current pulses (0.2 ms in duration) were delivered by the data acquisition software (Mobius; Panasonic, Alpha-Med Sciences) at 0.017 Hz through the selected stimulating microelectrode. The fEPSPs recorded at the remaining microelectrodes were amplified by a 64-channel amplifier, displayed on the monitor screen, and stored on the hard disk of a microcomputer for offline analysis. For LTP induction, after the baseline synaptic responses were stabilized for at least 30 min, a theta burst stimulation (TBS) protocol (5 bursts at 5 Hz, repeated 5 times at 10 s intervals, 4 pulses at 100 Hz for each burst) was delivered with the stimulation intensity eliciting 40%–60% of the maximum response (Li et al., 2010; Song et al., 2017; Ko et al., 2018). For LTD induction, stable baseline responses were recorded for at least 20 min before delivery of the low-frequency stimulation (LFS) protocol (1 Hz, 900 pulses) (Liu and Zhuo, 2014). To test the effects of channel inhibitors on LTP induction, the ASIC1a inhibitor PcTx1 (100 nM) was applied from 15 min before until 15 min after the TBS delivery. For LFS-LTD, PcTx1 or another ASIC1a channel inhibitor compound 5b (100 nM) was applied from 15 min before LFS and maintained continuously during the LFS. All multichannel electrophysiological data were analyzed offline by the MED64 Mobius software. For quantification of LTP and LTD data, the slope of fEPSPs was measured, normalized, and expressed as percentage change from the baseline level. The numbers of activated channels versus LTP-showing or LTD-showing channels were counted, and the induction ratios of cingulate LTP/LTD were calculated as follows: (number of LTP- or LTD-showing channels/number of all activated channels) × 100% (Li et al., 2016; Liu et al., 2016).

Experimental design and statistical analysis. Before the start of experiments, all animals were acclimatized to their environment for at least 1 week. Mice were assigned to different groups randomly in pharmacological and genetic studies. All behavioral tests were conducted in a temperature-controlled room by an experimenter blinded to the identity of drug treatment and/or mouse genotype. Group sample size was chosen on the basis of previous studies using the same methodologies. Animals with incorrect viral injections or cannula locations were excluded from

final analyses. All immunoblotting experiments were repeated at least three times with similar results. Prism software (GraphPad 6.0; RRID: SCR_002798) was used to conduct the statistical analysis. Data distribution was assumed to be normal, but this was not formally tested. The variance between the groups that are being statistically compared is similar. For every figure, statistical tests are justified as appropriate. Tests for statistical differences between groups were performed using Student's *t* test or a one-way ANOVA or two-way repeated-measures ANOVA followed by Tukey's or Sidak's *post hoc* test as described in the text. All data are presented as the mean ± SEM. In all cases, $p < 0.05$ was considered statistically significant.

Results

Manipulations of ASIC1a in ACC affect pain hypersensitivity

Before dissecting the function of ASIC1a in ACC, we first analyzed the expression of ASIC1a in the ACC. Western blot analysis showed that ASIC1a protein was highly enriched in ACC, comparable with the amounts in olfactory bulb and insular cortex (ACC: $t_{(3)} = 6.455$, $p = 0.0075$ vs hippocampus; insular cortex: $t_{(3)} = 3.932$, $p = 0.0293$ vs hippocampus; amygdala: $t_{(3)} = 6.740$, $p = 0.0067$ vs hippocampus; Student's *t* test; Fig. 1*A*). To confirm the functional expression of ASIC1a in ACC neurons, we measured ASIC1a-mediated synaptic response in neurons of superficial layer (layer II-III) of ACC slices evoked by stimulating deep layer (layer V-VI) at an intensity of 40 μA under whole-cell voltage-clamp mode. After blocking AMPARs and NMDARs, respectively, with CNQX (20 μM) and D-APV (50 μM), a small component of the EPSC remained in WT neurons (19.9 ± 2.1 pA, $n = 7$ neurons/3 mice). This was significantly inhibited by amiloride (200 μM), a nonselective ASIC blocker (Du et al., 2014), and PcTx1 (100 nM), a selective ASIC1a inhibitor (Escoubas et al., 2000) (amiloride: 3.26 ± 1.2 pA, $n = 7$ neurons/3 mice, $t_{(6)} = 8.185$, $p = 0.0002$ vs CNQX + APV, paired Student's *t* test; PcTx1: 4.19 ± 1.3 pA, $n = 8$ neurons/3 mice, $t_{(7)} = 6.791$, $p = 0.0003$ vs CNQX + APV, paired Student's *t* test; Fig. 1*B*). Similarly, the residual current in the presence of D-APV and CNQX was largely lacking in ASIC1a KO neurons (3.94 ± 1.4 pA, $n = 7$ neurons/4 mice, $t_{(12)} = 6.225$, $p = 0.00004$ vs WT, unpaired Student's *t* test; Fig. 1*B*). To exclude the possibility that the residual current might be due to less complete blockade of NMDARs by the relatively low dose of D-APV, we repeated the above recordings using a higher dose of D-APV (100 μM) and CNQX (20 μM). However, the amiloride-sensitive synaptic current was still readily detected (EPSC amplitude after CNQX+APV: 28.9 ± 2.2 pA; EPSC amplitude after CNQX + APV + amiloride: 2.8 ± 2.1 pA; $n = 7$ neurons/4 mice, $t_{(6)} = 4.831$, $p = 0.0029$, paired Student's *t* test). To examine whether the ASIC1a-mediated EPSC in the ACC is intensity-dependent, we performed electrophysiological recordings with a lower baseline stimulation intensity (10 μA). Interestingly, the amiloride-sensitive current became insignificant in the presence of CNQX and APV (EPSC amplitude after CNQX+APV: 4.5 ± 1.8 pA; EPSC amplitude after CNQX + APV + amiloride: 2.6 ± 1.2 pA; $n = 7$ neurons/4 mice, $t_{(6)} = 1.167$, $p = 0.2874$, paired Student's *t* test). These results demonstrate that, similar to previous observations in other brain regions (Du et al., 2014; Kreple et al., 2014; Yu et al., 2018), ASIC1a contributes to synaptic transmission in the ACC, but only under high input stimulation intensities, which would be expected to release more protons into the synaptic cleft to induce ASIC1a activation.

Considering the previously reported role of ASIC1a in nociceptive modulation at peripheral and spinal levels (Bohlen et al., 2011; Diochot et al., 2012; Duan et al., 2012), we next evaluated whether ASIC1a in ACC also contributes to cortical pain processing. First, we examined the role of cingulate ASIC1a in inflammatory pain through the conditional gene deletion strategy by injecting AAV encoding Cre recombinase driven by the human synapsin I promoter for neuron-specific expression (AAV-hSyn-Cre) into ACC of ASIC1a$^{flox/flox}$ mice (Wu et al., 2013). The inflammatory pain model was established 1 month later by injecting CFA into mouse hindpaw (Fig. 1*C*). AAV-expressing GFP was used as the control (AAV-hSyn-Ctrl) (Fig. 1*D*). Immunostaining showed that almost all of the GFP-positive cells expressed the neuron marker, NeuN, indicating the specificity of virus infection in neurons (Fig. 1*E*,*F*). The effectiveness of AAV-hSyn-Cre was confirmed by Western blotting showing reduced ASIC1a expression in ACC compared with AAV-hSyn-Ctrl ($t_{(4)} = 12.34$, $p = 0.0002$, unpaired Student's *t* test; Fig. 1*G*). Notably, the conditional deletion of ASIC1a in ACC greatly attenuated CFA-induced thermal ($F_{(1,7)} = 38.13$, $p = 0.0005$, two-way repeated-measures ANOVA; Tukey's multiple-comparison test: day 1: $p = 0.0001$; day 3: $p = 0.0011$; day 5: $p = 0.0065$; day 7: $p = 0.0123$; Fig. 1*H*) and mechanical hypersensitivity ($F_{(1,7)} = 15.58$, $p = 0.0056$, two-way repeated-measures ANOVA; Tukey's multiple-comparison test: day 1: $p = 0.0102$; day 3: $p = 0.0027$; day 5: $p = 0.0252$; day 7: $p = 0.0137$; Fig. 1*I*), implicating an important contribution of cingulate ASIC1a in inflammatory pain.

As an alternative approach to eliminate ASIC1a expression, we generated AAV encoding an shRNA for ASIC1a, driven by the U6 promoter. AAV-ASIC1a-shRNA or a negative control virus (AAV-NC-Ctrl) was injected bilaterally in ACC of WT mice (Fig. 1*J–L*). The shRNA-mediated knockdown of ASIC1a in ACC also alleviated inflammatory pain hypersensitivity (thermal: $F_{(1,7)} = 47.82$, $p = 0.0002$, two-way repeated-measures ANOVA; Tukey's multiple-comparison test: day 1: $p = 0.0025$; day 3: $p = 0.0165$; day 5: $p = 0.0440$; day 7: $p = 0.2949$; Fig. 1*M*; mechanical: $F_{(1,7)} = 9.83$, $p = 0.0165$, two-way repeated-measures ANOVA; Tukey's multiple-comparison test: day 1: $p = 0.0426$; day 3: $p = 0.0277$; day 5: $p = 0.0439$; day 7: $p = 0.3250$; Fig. 1*N*). Together, these results support a specific role for ACC-expressed ASIC1a in the development of inflammation-induced pain hypersensitivity.

In addition to genetic manipulation of ASIC1a expression, we also pharmacologically blocked ASIC1a activation by injecting PcTx1 bilaterally into ACC (10 μM, 0.5 μl per side), on the day before, during, and 1 d after the CFA injection (Fig. 2*A*,*B*). The treatment with PcTx1 prevented development of inflammatory thermal hyperalgesia compared with the saline control ($F_{(1,9)} = 24.9$, $p = 0.0007$, two-way repeated-measures ANOVA; Tukey's multiple-comparison test: day 1: $p = 0.0001$; day 3: $p = 0.00005$; day 5: $p = 0.0056$; day 7: $p = 0.1450$; Fig. 2*C*). Control experiments showed that PcTx1 had no effect on basal nociception, locomotor ability, and anxiety-related emotional state of naive mice (Fig. 2*D–I*). Thus, pharmacological blockade of ASIC1a yielded similar results as genetic deletion of ASIC1a gene, pointing to the importance of cingulate ASIC1a function in inflammatory pain.

ASIC1a is required for LTP induction in ACC

ASIC1a-mediated synaptic plasticity plays pivotal physiological roles in specific brain regions, such as spatial memory in hippocampus and conditioned taste aversion in insular cortex (Wemmie et al., 2002; Li et al., 2016). Meanwhile, LTP in ACC is considered as a critical cellular mechanism of chronic pain (Bliss et al., 2016). Thus, we hypothesized that ASIC1a may contribute to inflammatory pain hypersensitivity through regulation of ACC LTP. To test this hypothesis, we evaluated the role of

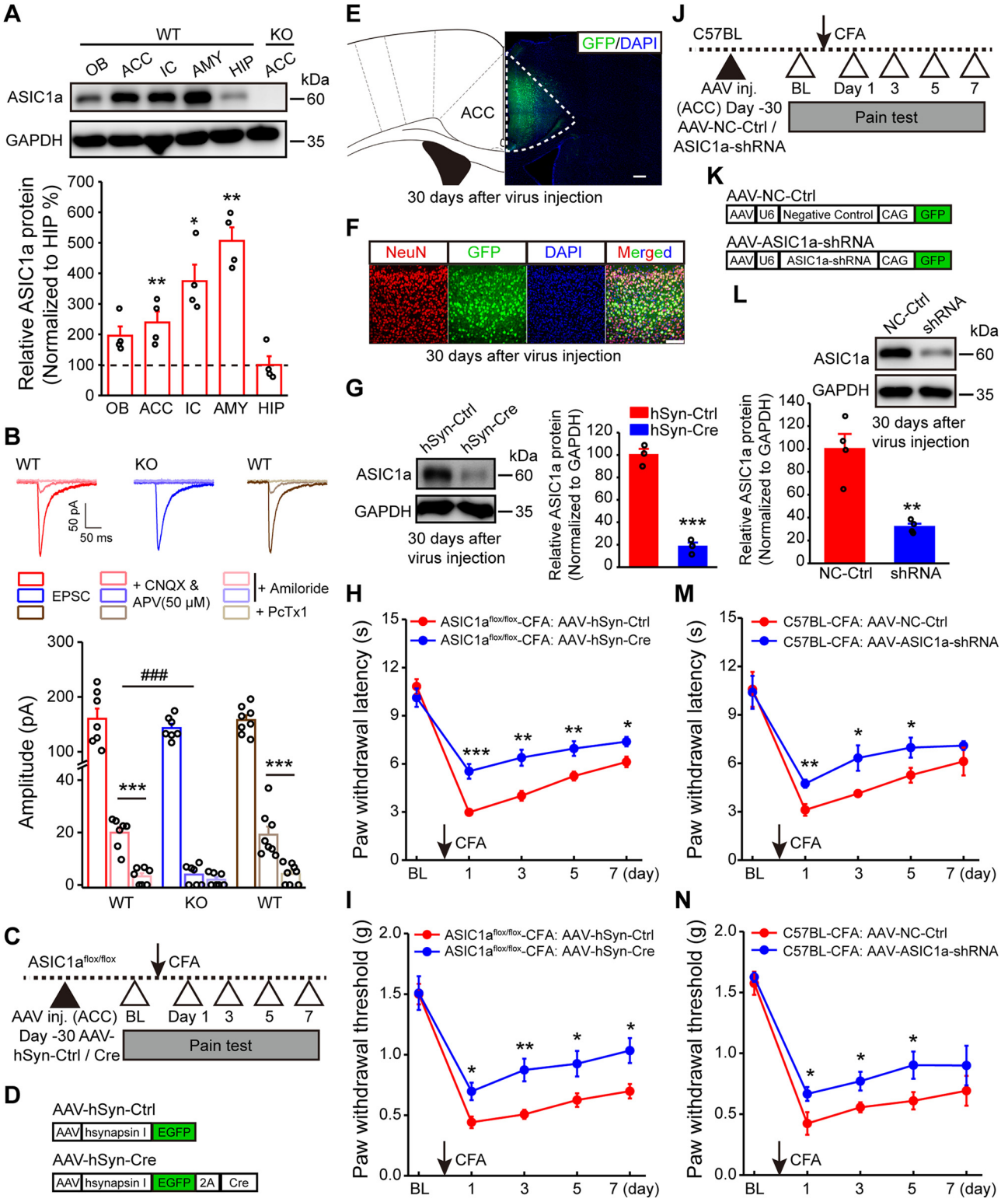

Figure 1. Genetic manipulations of ASIC1a in ACC influence inflammatory pain hypersensitivity. ***A***, Representative images and quantification of Western blots showing ASIC1a protein enrichment in ACC and several other brain regions. Data represent optical density values normalized to that of hippocampus. $n = 4$ mice. OB, Olfactory bulb; IC, insular cortex; AMY, amygdala; HIP, hippocampus. ***B***, Representative traces of EPSCs recorded with a high basal stimulation intensity before and after APV (50 μM) + CNQX, and after amiloride or PcTx1 in WT or ASIC1a KO mice. Bottom, Quantification of the ASIC-mediated synaptic currents. $n = 7$ or 8 neurons/3 mice for WT; $n = 7$ neurons/4 mice for ASIC1a KO. ***C***, Schematic diagram of experimental procedure for conditional deletion experiments. ***D***, Schematic illustration of the viral vectors for AAV-hSyn-Ctrl and AAV-hSyn-Cre. ***E***, Confocal image showing efficient expression of AAV-hSyn-Cre in ACC of an ASIC1a $^{flox/flox}$ mouse. Scale bar, 200 μm. ***F***, Colabeling of virus-derived GFP with the neuronal marker NeuN. Scale bar, 100 μm. ***G***, Representative images and quantification of Western blots showing that AAV-hSyn-Cre injection reduced ASIC1a expression in ACC ($n =$ 3 mice per group). ***H***, ***I***, ACC-specific deletion of ASIC1a significantly attenuated CFA-evoked thermal hyperalgesia (***H***) and mechanical allodynia (***I***). $n = 8$ mice for each group. ***J***, Schematic diagram of experimental procedure for knockdown experiments. ***K***, Schematic illustration of the viral vectors for AAV-NC-Ctrl and AAV-ASIC1a-shRNA. ***L***, Representative images and quantification of Western blots showing that AAV-ASIC1a-shRNA injection reduced ASIC1a expression in ACC ($n = 4$ mice per group). ***M***, ***N***, Genetic knockdown of ASIC1a in ACC produced significant analgesic effects in thermal (***M***) and mechanical (***N***) pain tests. $n = 8$ mice per group. BL, Baseline; Ctrl, control. Data are mean ± SEM. $^{*}p < 0.05$, $^{**}p < 0.01$, $^{***}p < 0.001$, $^{\#\#\#}p < 0.001$.

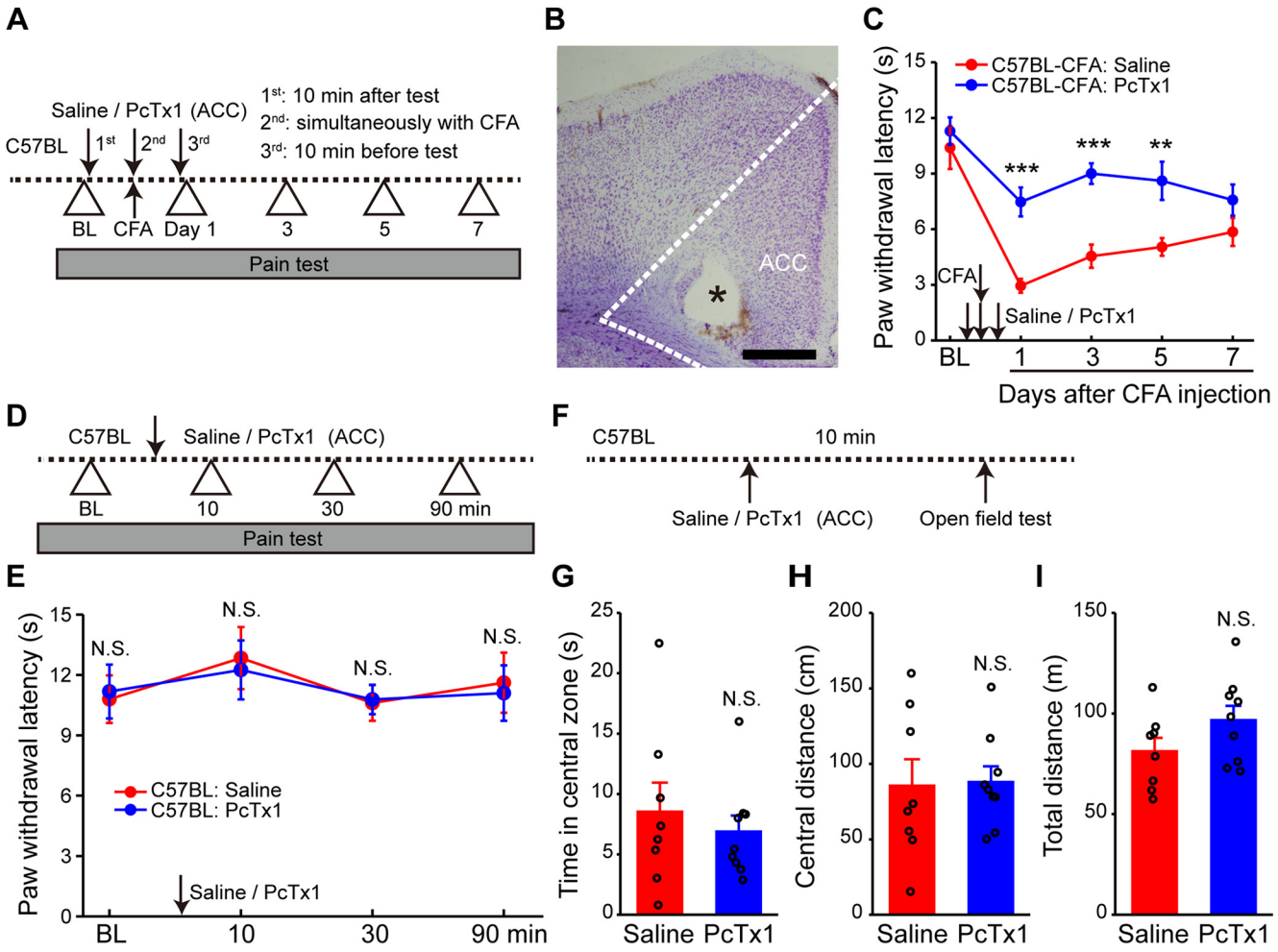

Figure 2. Pharmacological manipulations of ASIC1a in ACC affect inflammatory pain hypersensitivity. ***A***, Schematics of the experimental protocol for ***C***. The animals were pretreated with the selective ASIC1a blocker, PcTx1, injected in ACC. CFA-induced inflammatory pain was then behaviorally assessed. ***B***, Example Nissl-stained image depicting the location of the injection cannula (indicated by the asterisk). Scale bar, 500 μm. ***C***, PcTx1 pretreatment prevented CFA-evoked thermal hyperalgesia. $n = 10$ mice for each group. ***D***, Schematics of the experimental protocol for ***E***. ***E***, PcTx1 did not affect normal heat nociception ($n = 8$ mice per group). ***F***, Schematics of the experimental protocol for ***G–I***. ***G–I***, Open field test showing no difference between saline- and PcTx1-treated groups in the time spent in the center zone (***G***), distance traveled in the center arena (***H***), or total distance traveled (***I***) (saline group, $n = 8$ mice; PcTx1 group, $n = 9$ mice). Data are mean ± SEM. $^{**}p < 0.01$, $^{***}p < 0.001$, N.S., not significant.

ASIC1a in cingulate LTP inducibility. First, we showed that global deletion of ASIC1a did not significantly alter basal synaptic transmission and intrinsic membrane excitability of ACC neurons (Fig. 3). Neither input-output curve of AMPAR-mediated EPSC (Fig. 3*F*,*G*) nor the mEPSC frequency/amplitude (Fig. 3*L–N*) was altered by ASIC1a KO. There was equally no significant change in the presynaptic neurotransmitter release probability as demonstrated by the lack of any effect on paired-pulse ratio (Fig. 3*H*,*I*). In particular, we did not detect any significant change in AMPAR/NMDAR ratio in the ASIC1a KO mice (Fig. 3*J*,*K*), suggesting no apparent alteration of NMDAR currents after genetic deletion of ASIC1a.

We next examined the possible involvement of ASIC1a in LTP induction, using a previously established 64-channel multielectrode array (MED64) recording system (Liu et al., 2016). The relative position of the MED64 probe with an ACC slice is exemplified in Figure 4*A*. An electrode channel (Fig. 4*A*, right, red dot) was chosen to deliver electrical stimulation in the deep layer of the ACC slice, whereas those other channels of the 64-channel array that could reliably detect clear fEPSPs were assumed to be recording sites. These are referred to as activated channels. With the application of TBS from the stimulation channel, the percentage of activated channels that developed LTP, defined as LTP induction ratio (see Materials and Methods), reached 75.2 ± 5.3% in slices from control ASIC1a$^{flox/flox}$ mice injected with AAV-hSyn-Ctrl (Fig. 4*B*,*C*). Remarkably, with conditional deletion of ASIC1a in ACC (AAV-hSyn-Cre-injected), the LTP induction ratio greatly reduced to 29.4 ± 8.0% ($t_{(10)} = 4.784$, $p = 0.0007$ vs AAV-hSyn-Ctrl, unpaired Student's *t* test; Fig. 4*C*).

To confirm that the impaired ACC LTP indeed resulted from the loss of ASIC1a in ACC, we injected AAV driven by the human synapsin I promoter for neuron-specific ASIC1a overexpression (AAV-hSyn-ASIC1a) into ACC of adult ASIC1a KO mice. Intra-ACC injection of AAV-hSyn-ASIC1a, but not AAV-hSyn-Ctrl, successfully rescued LTP (Fig. 4*D*), with the induction ratio increased from 32.4 ± 3.6% for AAV-hSyn-Ctrl to 81.1 ± 5.6% for AAV-hSyn-ASIC1a ($t_{(13)} = 7.451$, $p < 0.0001$ vs AAV-hSyn-Ctrl, unpaired Student's *t* test; Fig. 4*E*). Aside from genetic manipulations, we also performed pharmacological experiments and found that bath application of either PcTx1 (100 nM) or another ASIC1a inhibitor, compound 5b (100 nM) (Buta et al., 2015), blocked cingulate LTP induction (Fig. 4*F*,*G*). These results further substantiate that ASIC1a function is crucial for cingulate LTP induction.

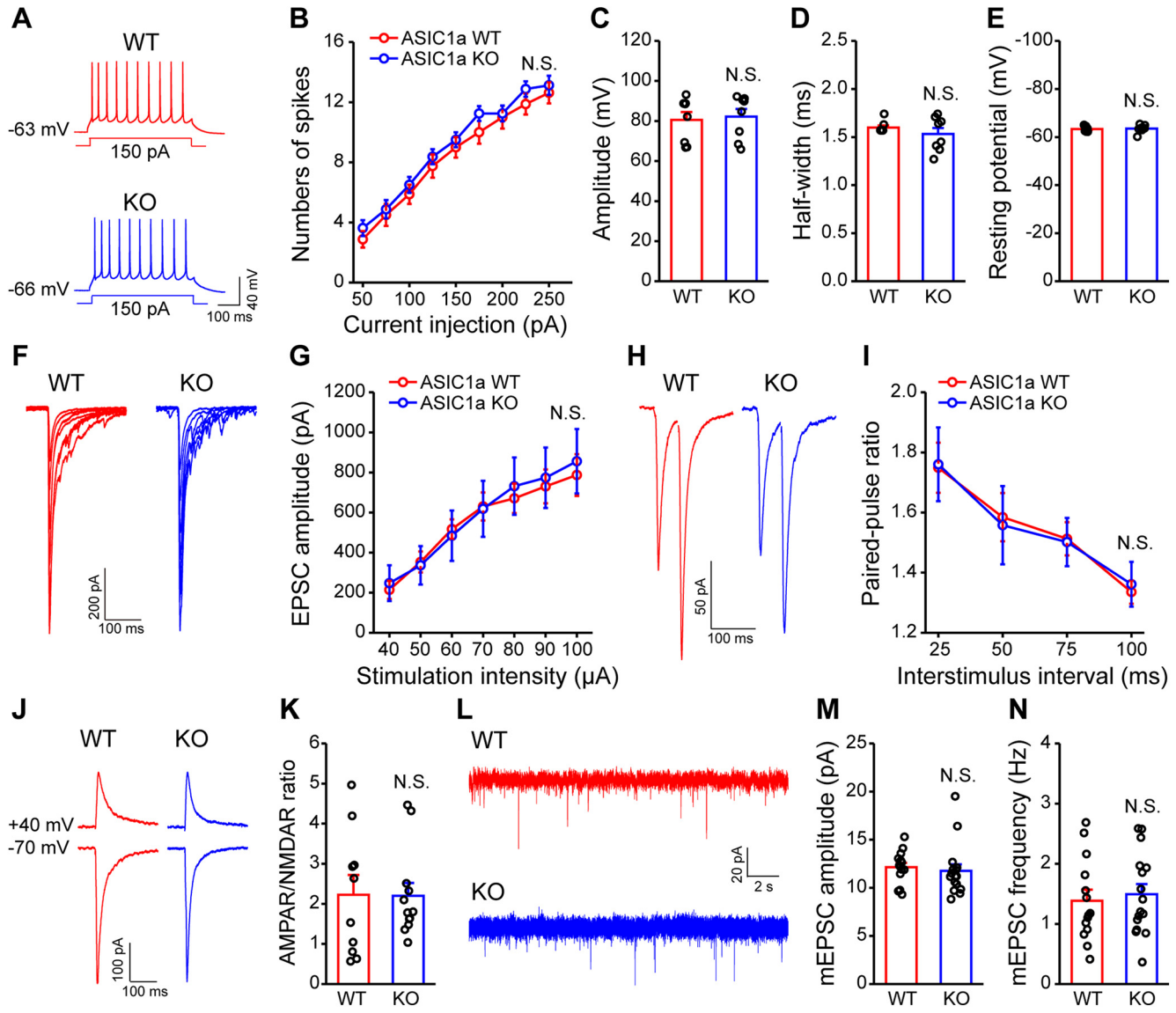

Figure 3. Intrinsic membrane properties and baseline synaptic transmission are unaltered in ACC of ASIC1a KO mice. ***A–E***, Representative traces (***A***) and pooled data (***B–E***) showing no effect of ASIC1a deletion on action potential firing properties in ACC pyramidal neurons. ***B***, Intensity-dependent increase in number of spikes elicited in ACC. ***C***, Action potential amplitude. ***D***, Action potential half-width. ***E***, Resting membrane potential of ACC neurons in ASIC1a WT and KO mice ($n = 8$ neurons/3 or 4 mice). ***F***, ***G***, Representative traces (***F***) and quantification of evoked EPSCs (***G***) showing no effect of ASIC1a deletion on input-output relationship of excitatory synaptic transmission in ACC ($n = 8$ neurons/4 mice). ***H***, ***I***, Representative plots (***H***) and quantification (***I***) of paired-pulse ratio recordings showing no effect of ASIC1a deletion on the probability of presynaptic neurotransmitter release ($n = 9–11$ neurons/4 or 5 mice). ***J***, ***K***, Representative traces (***J***) and quantification (***K***) of AMPAR/NMDAR ratios in ACC demonstrating no effect of ASIC1a deletion ($n = 10–12$ neurons/3 mice). ***L–N***, Representative traces (***L***) and quantification (***M***,***N***) revealing no obvious difference in the amplitude (***M***) or frequency (***N***) of mEPSCs recorded in ACC pyramidal neurons ($n = 14–16$ neurons/4 or 5 mice). Data are mean ± SEM. N.S., not significant.

ASIC1a is not required for LTD induction in ACC

We next investigated the effect of ASIC1a deletion/inhibition on cingulate LTD, another form of synaptic plasticity induced by LFS (Liu and Zhuo, 2014). With the conditional KO of ASIC1a in ACC of ASIC1a$^{flox/flox}$ mice using AAV-hSyn-Cre, LTD was still induced by LFS with an induction ratio of 79.0 ± 8.8%, which did not differ significantly from the AAV-hSyn-Ctrl-injected ASIC1a$^{flox/flox}$ mice (77.1 ± 0.5%, $t_{(8)} = 0.2215$, $p = 0.8303$ vs AAV-hSyn-Ctrl, unpaired Student's t test; Fig. 4*H*,*I*). Consistently, inhibiting ASIC1a function with PcTx1 or 5b also failed to prevent LFS-induced cingulate LTD (Fig. 4*J*,*K*). Together, these findings indicate that ASIC1a selectively regulates the inducibility of LTP in ACC, without affecting LTD.

ASIC1a in excitatory neurons of ACC is the major player in LTP and pain hypersensitivity

The aforementioned results show an important role of ASIC1a in the cingulate LTP and behavioral sensitization to peripheral inflammation. We next asked whether there is any cell type-related difference for the involvement of ASIC1a in pain hypersensitivity. Previous optogenetic studies have revealed that excitatory neurons are main contributors in ACC that modulate pain perception (Kang et al., 2015; Sellmeijer et al., 2018). Therefore, we first specifically knocked out ASIC1a in ACC excitatory neurons, by injecting AAV driven by the CaMKII promoter for excitatory neuron-specific Cre recombinase expression (AAV-CaMKII-Cre) into the ACC of ASIC1a$^{flox/flox}$ mice (Fig. 5*A*,*B*). The AAV-CaMKII-EGFP served as a control (AAV-CaMKII-Ctrl).

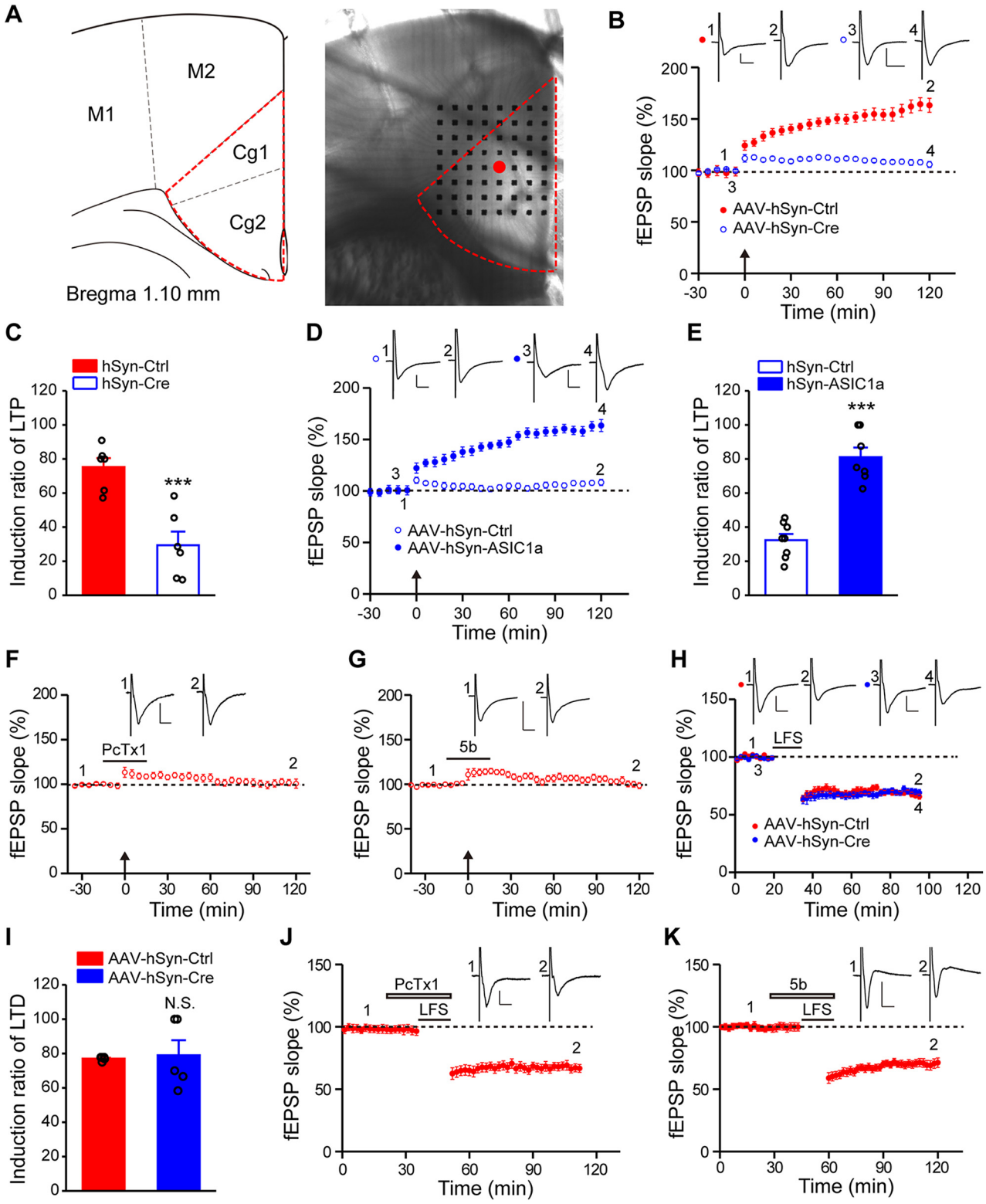

Figure 4. ASIC1a is selectively involved in LTP induction in ACC. ***A***, Left, Schematic diagram showing the location of ACC being studied. Right, Light microscopy photograph showing placement of the MED64 probe relative to the ACC slice. Red dot indicates the stimulation site where regular electrical stimuli were delivered to the deep layer of ACC. ***B***, ***C***, Conditional deletion of ASIC1a in ACC neurons reduced the induction probability of LTP ($n = 6$ slices/6 mice). ***B***, Summary plot of fEPSP slopes showing impaired LTP in the ASIC1a conditional KO mice. ***C***, Induction ratios of cingulate LTP, calculated using the following formula: (number of LTP-showing channels/number of all activated channels) × 100%. ***D***, ***E***, Expression of exogenous ASIC1a in ACC rescued cingulate LTP induction in ASIC1a null mice ($n = 7$ or 8 slices/4 or 5 mice). ***F***, ***G***, Summary plot of fEPSP slopes showing impairment of LTP induction in ACC treated with ASIC1a blockers, PcTx1 (***F***, $n = 6$ slices/6 mice), and compound 5b (***G***, $n = 6$ slices/6 mice). ***B***, ***D***, ***F***, ***G***, Insets, Representative fEPSP traces at the time points indicated by numbers in the graph. Calibration: 100 μV, 10 ms. Arrows indicate the TBS application. ***H***, Summary plot of fEPSP slopes showing comparable induction of cingulate LTD in control and conditional ASIC1a KO mice ($n = 5$ slices/5 mice). ***I***, Induction ratios of LTD. ***J***, ***K***, Bath application of PcTx1 (***J***, $n = 6$ slices/5 mice) or compound 5b (***K***, $n = 5$ slices/5 mice) did not block LTD induction in ACC. ***H***, ***J***, ***K***, Insets, Representative fEPSP traces at the time points indicated. Calibration: ***H***, ***K***, 100 μV, 10 ms; ***J***, 50 μV, 10 ms. Horizontal bars represent the LFS or drug delivery as indicated. Data are mean ± SEM. ***$p < 0.001$, N.S., not significant.

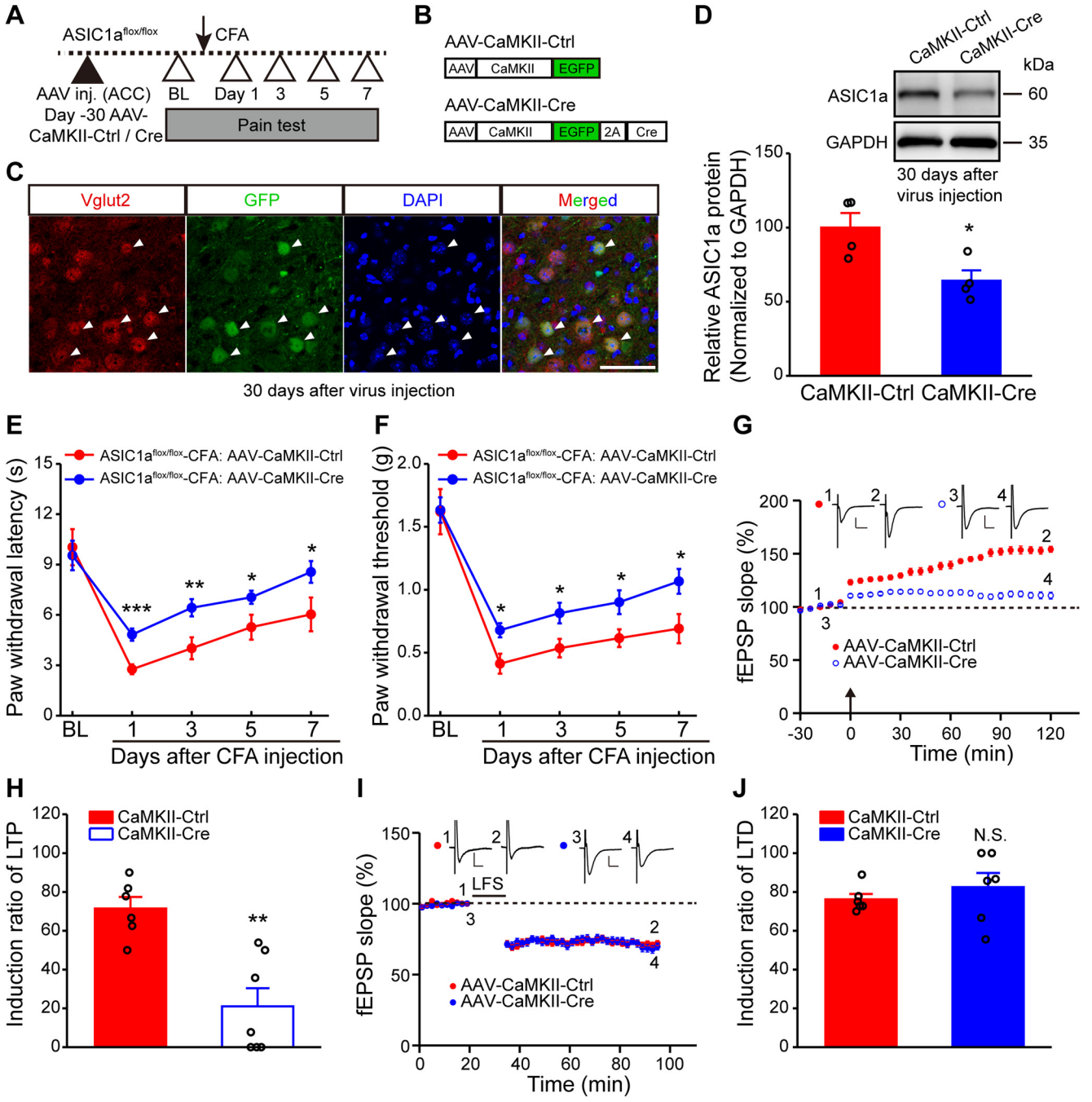

Figure 5. ASIC1a in excitatory neurons of ACC is the major contributor to cingulate LTP and behavioral hypersensitivity. ***A***, Schematic of the experimental procedure for excitatory neuron-specific ASIC1a deletion. ***B***, Schematic diagram of the viral vectors for AAV-CaMKII-Ctrl and AAV-CaMKII-Cre. ***C***, Confocal images showing the colocalization of GFP (i.e., the AAV-CaMKII-EGFP virus) and Vglut2 (excitatory neuronal marker) immunofluorescence. Filled arrowheads indicate the colabeled neurons. Scale bar, 50 μm. ***D***, Representative images and quantification of Western blots demonstrating that AAV-CaMKII-Cre injection reduces ASIC1a expression in ACC ($n = 4$ mice per group). ***E***, ***F***, Conditional deletion of ASIC1a in excitatory neurons significantly attenuated CFA-evoked thermal hyperalgesia (***E***) and mechanical allodynia (***F***). $n = 10$ mice for each group. ***G***, ***H***, Conditional deletion of ASIC1a in excitatory neurons reduced induction probability of cingulate LTP (***G***, summary plot of fEPSP slopes; ***H***, induction ratios of LTP). $n = 6$ or 7 slices/6 or 7 mice. ***I***, ***J***, LTD was not affected by ASIC1a deletion in excitatory neurons of ACC (***I***, summary plot of fEPSP slopes; ***J***, induction ratios of LTD). $n = 6$ slices/6 mice. ***G***, ***I***, Insets, Representative fEPSP traces at the time points indicated by numbers in the graph. Calibration: 100 μV, 10 ms. ***G***, Arrow indicates the TBS application. ***I***, Horizontal bar represents the LFS delivery to induce LTD. Data are mean ± SEM. $^*p < 0.05$, $^{**}p < 0.01$, $^{***}p < 0.001$, N.S., not significant.

Confocal imaging analysis showed that most GFP-positive cells colocalized with the marker of excitatory neurons, Vglut2, confirming the specificity of virus infection (Fig. 5*C*). Western blotting data demonstrated the significant reduction of ASIC1a protein expression in the conditionally deleted group compared with the control ($t_{(6)} = 2.98$, $p = 0.0246$, unpaired Student's t test; Fig. 5*D*). Behaviorally, the selective deletion of ASIC1a in ACC excitatory neurons significantly reduced CFA-evoked thermal and mechanical hypersensitivity (thermal: $F_{(1,9)} = 6.75$, $p = 0.0288$, two-way repeated-measures ANOVA; Tukey's multiple-comparison test: day 1: $p = 0.0003$; day 3: $p = 0.0097$; day 5: $p = 0.0483$; day 7: $p = 0.0489$; Fig. 5*E*; mechanical: $F_{(1,9)} = 12.26$, $p = 0.0067$, two-way repeated-measures ANOVA; Tukey's multiple-comparison test: day 1: $p = 0.0134$; day 3: $p = 0.0205$; day 5: $p =$

0.0266; day 7: $p = 0.0234$; Fig. 5*F*). Electrophysiologically, LTP induction ratio reduced from 71.5 ± 5.9% for AAV-CaMKII-Ctrl-injected to 21.0 ± 9.3% for AAV-CaMKII-Cre-injected ASIC1a$^{flox/flox}$ mice ($t_{(11)} = 4.389$, $p = 0.0011$, unpaired Student's *t* test; Fig. 5*G*,*H*). However, LTD was induced successfully with an induction ratio of 82.4 ± 7.3% in the AAV-CaMKII-Cre group, comparable with the control (76.2 ± 2.8%, $t_{(10)} = 0.7967$, $p = 0.4441$, unpaired Student's *t* test; Fig. 5*I*,*J*).

ASIC1a is required for chronic pain-induced membrane translocation of GluA1 in ACC

So far, the above results suggest that ASIC1a in excitatory neurons of the ACC contributes to inflammatory pain sensitization through promoting LTP of synaptic transmission. To explore the molecular mechanisms underpinning the involvement of ASIC1a in cingulate LTP and inflammatory pain, we first examined whether the expression of ASIC1a was upregulated in ACC after CFA injection. However, in contrast to our previous finding that CFA-induced inflammation resulted in increased expression of ASIC1a in dorsal horn of spinal cord (Wu et al., 2004), the total protein levels of ASIC1a remained unaltered at day 1, day 3, and day 7 after CFA injection (Fig. 6*A*,*B*). Yet, the amount of ASIC1a protein on the plasma membrane appeared to increase, suggesting an enhanced membrane trafficking of ASIC1a in response to CFA-induced peripheral inflammation ($t_{(8)} = 3.723$, $p = 0.0058$, WT-saline vs WT-CFA, unpaired Student's *t* test; Fig. 6*E*,*F*). Second, GluN2B, a critical subunit of NMDAR, has been shown to play critical roles in ACC LTP and chronic pain (Wu and Zhuo, 2009). We observed a significant increase in total protein levels of GluN2B, but not that of GluA1, in ACC of CFA-injected mice (GluN2B: $F_{(3,11)} = 4.47$, $p = 0.0276$, one-way ANOVA; Tukey's multiple-comparison test: WT-saline vs WT-CFA, $p = 0.0421$; Fig. 6*C*,*D*). However, this change was unaffected by ASIC1a deletion, suggesting that the upregulation of GluN2B was independent of ASIC1a (one-way ANOVA followed by Tukey's multiple-comparison test: KO-saline vs KO-CFA, $p = 0.0476$; Fig. 6*D*).

Another important step of cingulate LTP is AMPAR trafficking, which also plays a role in chronic pain (Toyoda et al., 2007). We next used subcellular fractionation (for details, see Materials and Methods) to examine the changes in membrane content of AMPARs in the ACC. A marked increase in the plasma membrane level of GluA1 subunit of AMPAR was detected following CFA-induced inflammation in WT mice, but not ASIC1a KO mice ($F_{(3,14)} = 5.34$, $p = 0.0116$, one-way ANOVA; Tukey's multiple-comparison test: WT-saline vs WT-CFA, $p = 0.0439$; KO-saline vs KO-CFA, $p = 0.6927$; Fig. 6*E*,*F*), suggesting that ASIC1a is critical for AMPAR trafficking to the membrane surface during CFA-induced inflammatory responses. Consistent with the biochemical findings, electrophysiological recordings showed an enhancement of AMPAR-mediated synaptic transmission in ACC 3 d after CFA injection, which was significantly attenuated by ASIC1a gene deletion ($F_{(3,21)} = 6.61$, $p = 0.0026$, two-way ANOVA; Tukey's multiple-comparison test: WT-saline vs WT-CFA, $p = 0.0400$, $p = 0.0015$, $p = 0.0026$, and $p = 0.0011$ for 70, 80, 90, and 100 μA, respectively; KO-saline vs KO-CFA, $p = 0.0190$, $p = 0.0018$, $p = 0.0021$, and $p = 0.0026$ for 70, 80, 90, and 100 μA, respectively; WT-CFA vs KO-CFA, $p = 0.0422$, $p = 0.0385$, and $p = 0.0325$ for 80, 90, and 100 μA, respectively; Fig. 6*G*,*H*). The postsynaptic mechanism of ASIC1a-dependent upregulation of AMPAR function was validated through the measurement of mEPSCs in ACC neurons. Whereas ACC of WT mice exhibited increases in both frequency and amplitude of mEPSCs after peripheral inflammation (mEPSC frequency: $F_{(3,28)} = 6.29$, $p = 0.0021$, one-way ANOVA; Tukey's multiple-comparison test: WT-saline vs WT-CFA, $p = 0.0069$; Fig. 6*I*,*J*; mEPSC amplitude: $F_{(3,28)} = 3.78$, $p = 0.0215$, one-way ANOVA; Tukey's multiple-comparison test: WT-saline vs WT-CFA, $p = 0.0146$; Fig. 6*I*,*K*), the ACC of ASIC1a KO mice only acquired an increase in mEPSC frequency, but not amplitude (one-way ANOVA followed by Tukey's multiple-comparison test: KO-saline vs KO-CFA, mEPSC frequency, $p = 0.0108$; mEPSC amplitude, $p = 0.5830$; Fig. 6*I*–*K*). Furthermore, CFA-induced decrease in paired-pulse ratio did not differ between WT and ASIC1a KO groups (Fig. 6*L*,*M*), indicating that ASIC1a was not required for pain-related enhancement of presynaptic transmitter release. Together, these results implicate that ASIC1a contributes to CFA-induced increase in GluA1 membrane trafficking in ACC and thereby enhances excitatory synaptic strength and nociceptive sensitivity.

ASIC1a works through PKCλ to promote LTP and pain hypersensitivity

Next, we examined the downstream signaling molecules required for ASIC1a-dependent GluA1 membrane trafficking and LTP induction. The atypical PKC isoforms, including PKCλ and PKMζ, have been reported to play critical roles in the initiation and maintenance of hippocampal LTP, respectively (Wang et al., 2016). Interestingly, atypical PKC isoforms are also involved in the pathogenesis of chronic pain (Li et al., 2010; Marchand et al., 2011). Because the electrophysiological data showed an induction deficit in the early phase of cingulate LTP following ASIC1a deletion (Fig. 4*B*), we explored the possibility that PKCλ is the missing link between ASIC1a and AMPAR tracking during cingulate LTP. We first checked whether PKCλ activation was affected in the ACC after peripheral inflammation and whether such an effect required ASIC1a. Three days after saline or CFA injection, ACC tissues were collected and subjected to Western blotting analysis, which showed an increase in the phosphorylation levels of PKCλ, without any detectable change in total expression of PKCλ. Importantly, ASIC1a deletion blocked the CFA-induced increase in PKCλ phosphorylation ($F_{(3,20)} = 2.523$, $p = 0.0368$, one-way ANOVA; Tukey's multiple-comparison test: WT-saline vs WT-CFA, $p = 0.0427$; KO-saline vs KO-CFA, $p = 0.7440$; Fig. 7*A*,*B*), indicating that the phosphorylation of PKCλ in ACC during inflammatory pain proceeds in an ASIC1a-dependent manner.

We then generated AAV constructs that express a PKCλ-targeting shRNA, AAV-PKCλ-shRNA, and a negative control virus (AAV-NC-Ctrl), and injected the virus bilaterally in ACC of WT mice (Fig. 7*C*,*D*). One month after viral injection, the levels of PKCλ and its phosphorylated form were significantly decreased in ACC (PKCλ: $t_{(4)} = 3.373$, $p = 0.0280$, unpaired Student's *t* test; p-PKCλ: $t_{(4)} = 2.84$, $p = 0.0469$, AAV-NC-Ctrl vs AAV-PKCλ-shRNA, unpaired Student's *t* test; Fig. 7*E*,*F*). Intriguingly, CFA-induced thermal hyperalgesia and mechanical allodynia were also dramatically attenuated (thermal: $F_{(1,15)} = 21.47$, $p = 0.0003$, two-way repeated-measures ANOVA; Sidak's multiple-comparison test: day 1: $p = 0.0012$; day 3: $p = 0.0147$; day 5: $p = 0.0076$; day 7: $p = 0.0058$; mechanical: $F_{(1,15)} = 11.25$, $p = 0.0044$, two-way repeated-measures ANOVA; Sidak's multiple-comparison test: day 1: $p = 0.0074$; day 3: $p = 0.0137$; day 5: $p = 0.0084$; day 7: $p = 0.0259$; Fig. 7*G*,*H*). Moreover, the knockdown of PKCλ prevented the induction of cingulate LTP (Fig. 7*I*), with the induction ratio reduced to 23.7 ± 4.2% compared with the control group (77.9 ± 6.0%, $t_{(13)} = 7.518$, $p <$

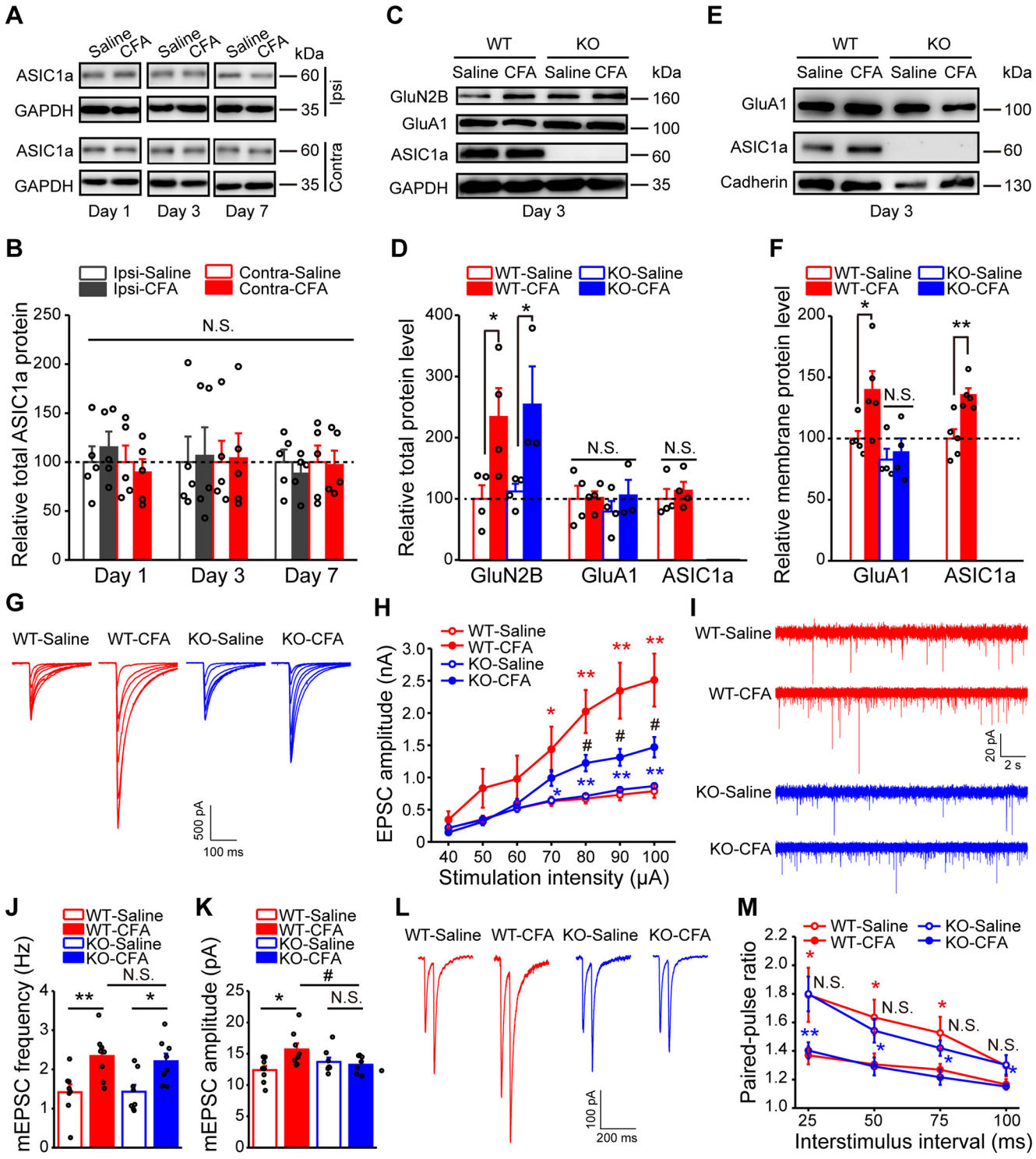

Figure 6. ASIC1a contributes to pain-related increase in membrane trafficking of AMPAR GluA1 subunit in ACC. ***A***, ***B***, Representative images (***A***) and quantification (***B***) of Western blots showing that CFA injection did not induce significant changes in the expression of total ASIC1a in ACC ($n = 5$ mice per group). Ipsi, Ipsilateral; Contra, contralateral. ***C***, ***D***, Representative images (***C***) and quantification (***D***) of Western blots showing that CFA injection evoked a strong ASIC1a-independent upregulation of total GluN2B expression in ACC (WT-saline, $n = 4$ mice; WT-CFA, $n = 4$ mice; KO-saline, $n = 4$ mice; KO-CFA, $n = 3$ mice). ***E***, ***F***, Representative images (***E***) and quantification (***F***) of Western blots showing that CFA injection induced a significant increase in the membrane content of GluA1 and ASIC1a in ACC (WT-saline, $n = 5$ mice; WT-CFA, $n = 5$ mice; KO-saline, $n = 4$ mice; KO-CFA, $n = 4$ mice). The CFA-evoked membrane trafficking of GluA1 was not detected in ACC of ASIC1a KO mice. Membrane fractions were prepared by subcellular fractionation for assessing GluA1 and ASIC1a levels in the plasma membrane. ***G***, ***H***, Representative traces (***G***) and quantification (***H***) of evoked EPSCs demonstrating that CFA injection enhanced AMPAR-mediated synaptic transmission in ACC, which was attenuated by ASIC1a deletion ($n = 8$ neurons/4 mice). ***I–K***, Representative traces (***I***) and quantification (***J***,***K***) of mEPSCs demonstrating that CFA injection resulted in increases in mEPSC frequency (***J***) and amplitude (***K***), and ASIC1a deletion blocked the change in mEPSC amplitude, but not frequency, in ACC neurons ($n = 8$ neurons/4 mice). ***L***, ***M***, Representative traces of paired-pulse ratio recording (***L***) and its quantification (***M***) demonstrating that ASIC1a is not involved in CFA-induced enhancement of presynaptic transmitter release (WT-saline, $n = 10$ neurons/5 mice; WT-CFA, $n = 12$ neurons/4 mice; KO-saline, $n = 11$ neurons/4 mice; KO-CFA, $n = 12$ neurons/5 mice). Data are mean ± SEM. $^{*}p < 0.05$ versus saline. $^{**}p < 0.01$ versus saline. $^{\#}p < 0.05$ versus WT, N.S., not significant.

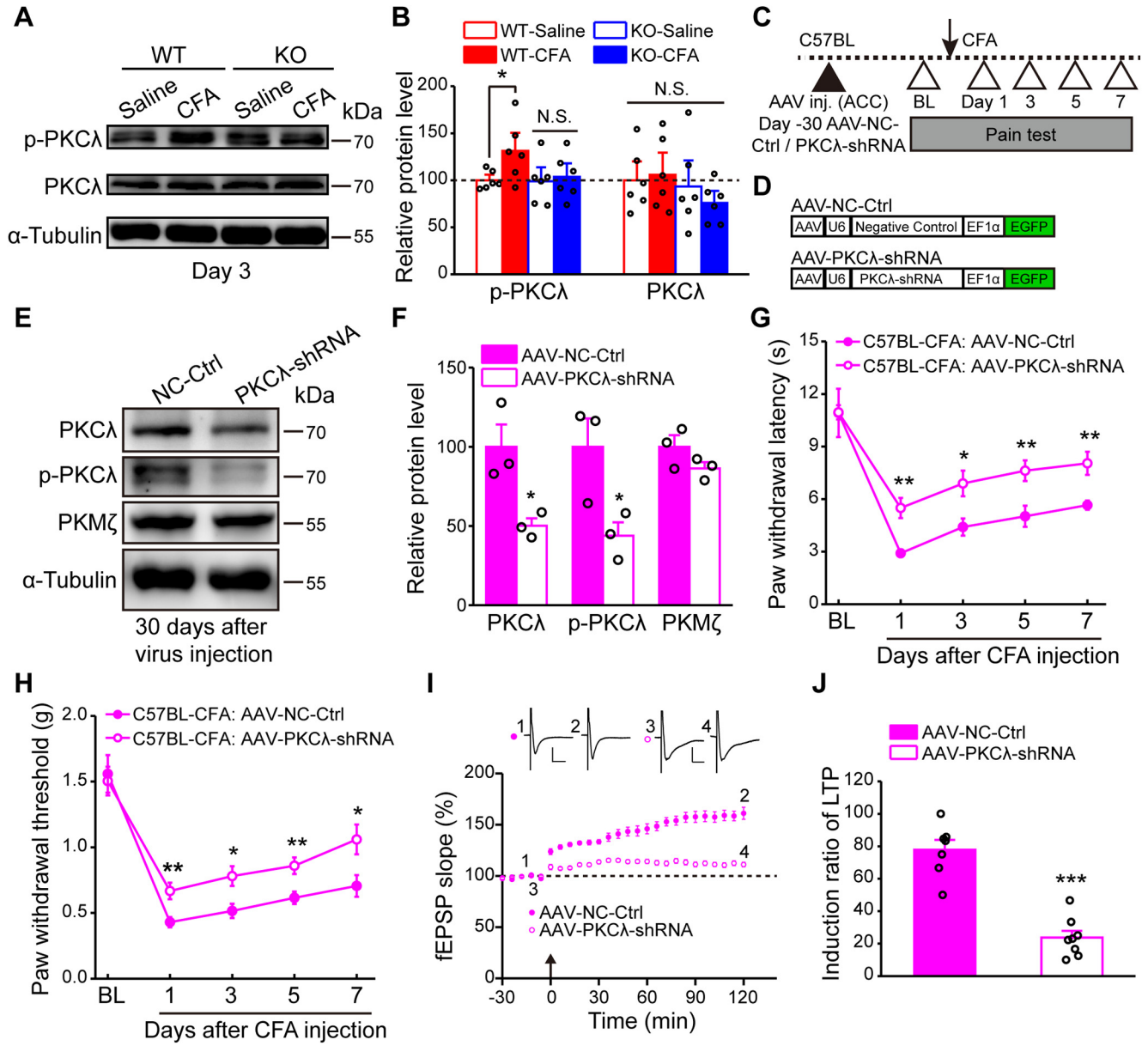

Figure 7. Genetic knockdown of PKCλ in ACC reduces inflammatory pain hypersensitivity and cingulate LTP. ***A***, ***B***, Representative images (***A***) and quantification (***B***) of Western blots showing that CFA injection induced a significant increase in the phosphorylation of PKCλ in ACC of WT but not that of ASIC1a KO mice ($n = 6$ mice per group). ***C***, Schematic of the experimental procedure for PKCλ knockdown. ***D***, Schematic diagram of the viral vectors for AAV-NC-Ctrl and AAV-PKCλ-shRNA. NC, Negative control. ***E***, ***F***, Representative images (***E***) and quantification (***F***) of Western blots demonstrating that AAV-PKCλ-shRNA injection significantly reduced the total and p-PKCλ levels in ACC ($n = 3$ mice per group). ***G***, ***H***, Genetic knockdown of PKCλ in ACC produced analgesic effects in both thermal (***G***) and mechanical (***H***) pain tests (AAV-NC-Ctrl, $n = 8$ mice; AAV-PKCλ-shRNA, $n = 9$ mice). ***I***, ***J***, Knockdown of PKCλ in ACC neurons reduced the induction probability of LTP ($n =$ 7 or 8 slices/5 mice). ***I***, Summary plot of fEPSP slopes. Insets, Representative fEPSP traces at the time points indicated. Calibration: left, 50 μV, 10 ms; right, 100 μV, 10 ms. Arrow indicates the TBS application. ***J***, Induction ratios of cingulate LTP. Data are mean ± SEM. *$p < 0.05$, **$p < 0.01$, ***$p < 0.001$, N.S., not significant.

0.0001, unpaired Student's t test; Fig. 7*J*). These observations support the notion that PKCλ knockdown can mimic the effect of ASIC1a loss of function in reducing cingulate LTP and mitigating inflammatory pain.

To further strengthen the conclusion that PKCλ is an intermediator linking ACC ASIC1a to synaptic potentiation and behavioral sensitization, we tested whether overexpression of exogenous PKCλ in ACC could rescue the behavioral defects and impaired LTP in ASIC1a KO mice (Fig. 8*A*,*B*). Intra-ACC administration of AAV-hSyn-PKCλ resulted in a profound increase in the expression levels of both PKCλ and its phosphorylated form compared with AAV-hSyn-Ctrl (PKCλ: $t_{(6)} = 9.27$, $p =$ 0.0001, unpaired Student's t test; p-PKCλ: $t_{(6)} = 6.288$, $p =$ 0.0008, AAV-hSyn-Ctrl vs AAV-hSyn-PKCλ, unpaired Student's t test; Fig. 8*C*,*D*), which also successfully restored inflammatory pain hypersensitivity in ASIC1a null mice (thermal: $F_{(1,7)} =$ 17.78, $p = 0.0040$, two-way repeated-measures ANOVA; Tukey's multiple-comparison test: day 1: $p = 0.0090$; day 3: $p = 0.0183$; day 5: $p = 0.0208$; day 7: $p = 0.0164$; mechanical: $F_{(1,7)} = 8.81$, $p = 0.0209$, two-way repeated-measures ANOVA; Tukey's multiple-comparison test: day 1: $p = 0.0428$; day 3: $p = 0.0022$; day 5: $p = 0.0124$; day 7: $p = 0.0076$; Fig. 8*E*,*F*). Furthermore, after expressing the exogenous PKCλ, ACC LTP was fully recovered (Fig. 8*G*), with the induction ratio reaching 79.0 ± 6.2% in the ASIC1a KO mice, which is significantly higher than that achieved by the AAV-hSyn-Ctrl-injected group (27.2 ± 8.6%,

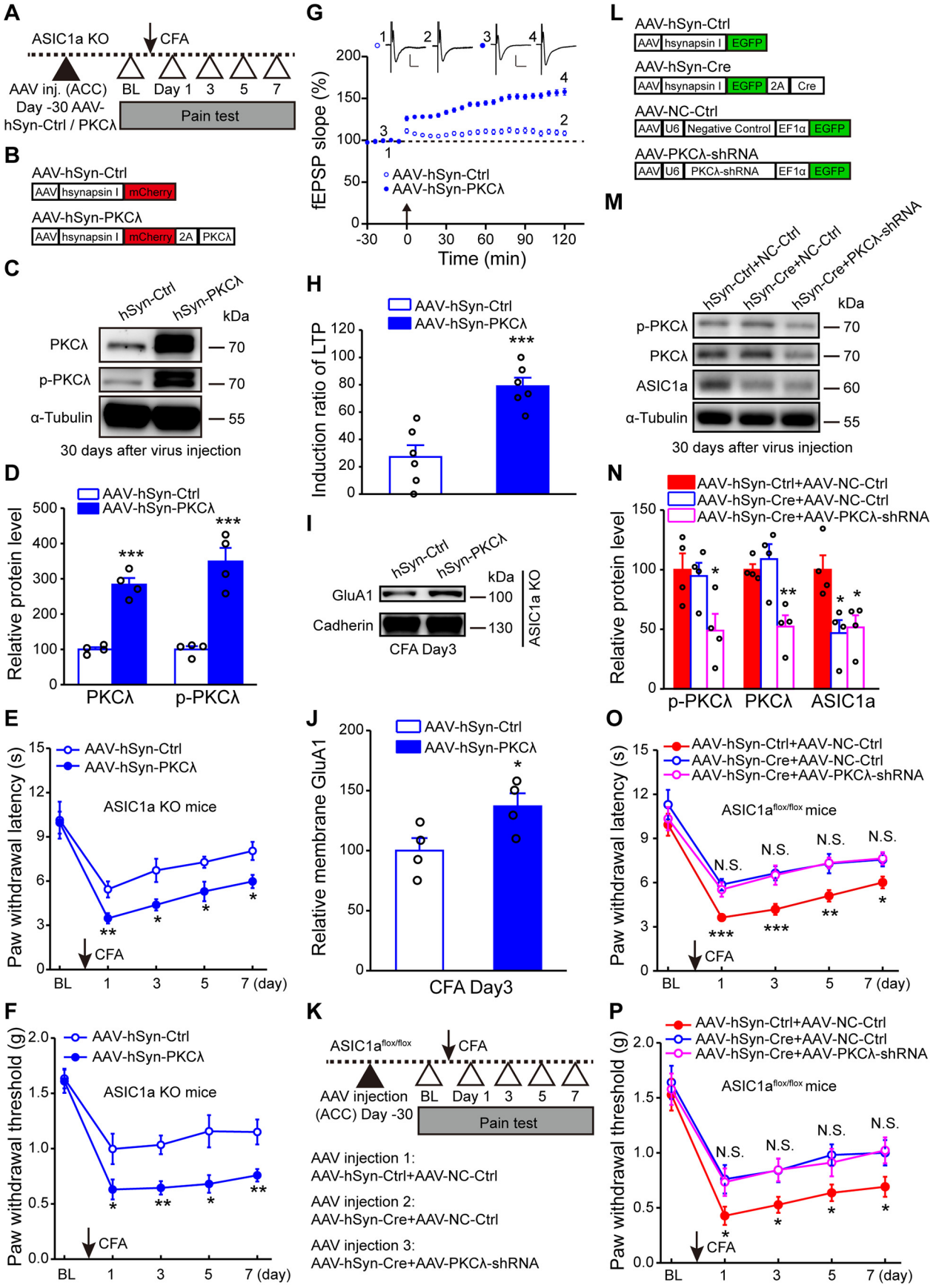

Figure 8. PKCλ mediates ASIC1a-dependent cortical LTP and inflammatory pain hypersensitivity. ***A***, Schematic of the experimental procedure for PKCλ overexpression. ***B***, Schematic diagram of the viral vectors for AAV-hSyn-Ctrl and AAV-hSyn-PKCλ. ***C***, ***D***, Representative images (***C***) and quantification (***D***) of Western blots demonstrating that AAV-hSyn-PKCλ injection enhanced expression and phosphorylation of PKCλ in ACC ($n = 4$ mice per group). ***E***, ***F***, Overexpression of PKCλ in ACC of ASIC1a KO mice recovered CFA-induced thermal hyperalgesia (***E***) and (*Figure legend continues.*)

$t_{(10)} = 4.879$, $p = 0.0006$, unpaired Student's t test; Fig. 8*H*). In the CFA-injected ASIC1a KO mice, AAV-hSyn-PKCλ also rescued the elevation of membrane GluA1 expression in ACC ($t_{(6)} = 2.453$, $p = 0.0496$, AAV-hSyn-Ctrl vs AAV-hSyn-PKCλ, unpaired Student's t test; Fig. 8*I*,*J*). To exclude the possibility that PKCλ and ASIC1a act parallelly, instead of sequentially, we examined the effect of PKCλ knockdown in the ASIC1a null background (Fig. 8*K*–*N*). We found that the simultaneous knockdown/KO of PKCλ and ASIC1a in ACC with the coinjection of AAV-PKCλ-shRNA and AAV-hSyn-Cre, respectively, in ASIC1a$^{flox/flox}$ mice did not further increase the thermal ($F_{(2,27)} = 12.73$, $p = 0.0001$, two-way repeated-measures ANOVA; Tukey's multiple-comparison test: AAV-hSyn-Ctrl + NC-Ctrl vs AAV-hSyn-Cre + NC-Ctrl, day 1: $p = 0.00007$; day 3: $p = 0.006$; day 5: $p = 0.0085$; day 7: $p = 0.0189$; AAV-hSyn-Cre + NC-Ctrl vs AAV-hSyn-Cre + PKCλ-shRNA, day 1: $p = 0.5984$; day 3: $p = 0.8742$; day 5: $p = 0.9561$; day 7: $p = 0.8948$; Fig. 8*O*) or mechanical ($F_{(2,27)} = 10.25$, $p = 0.0005$, two-way repeated-measures ANOVA; Tukey's multiple-comparison test: AAV-hSyn-Ctrl + NC-Ctrl vs AAV-hSyn-Cre + NC-Ctrl, day 1: $p = 0.0394$; day 3: $p = 0.0236$; day 5: $p = 0.0106$; day 7: $p = 0.0471$; AAV-hSyn-Cre + NC-Ctrl vs AAV-hSyn-Cre + PKCλ-shRNA, day 1: $p = 0.8842$; day 3: $p = 0.9767$; day 5: $p = 0.6648$; day 7: $p = 0.8945$; Fig. 8*P*) pain threshold compared with the conditional ASIC1a KO alone. These results indicate that the effects of ASIC1a and PKCλ on pain hypersensitivity are not additive. Therefore, a failure to activate PKCλ signaling in ACC represents the major deficit in the ASIC1a KO mice that leads to the diminished inflammatory pain and cingulate LTP.

ASIC1a induces PKCλ phosphorylation through intracellular Ca^{2+} increase

Next, we asked what might be the molecular mechanism linking ASIC1a activation to PKCλ phosphorylation in ACC. It has been shown that PKCλ activation relies on elevation of intracellular Ca^{2+}, which further triggers phosphoinositide 3-kinase activation (Suzuki et al., 2003; Ren et al., 2013). Here, we used primary cultures of cortical neurons to determine whether intracellular Ca^{2+} elevation caused by ASIC1a is involved in increasing PKCλ phosphorylation. First, we performed Ca^{2+} imaging experiments to show that application of the acidic, pH 6.0, solution elicited a rise in intracellular Ca^{2+} concentration in cultured mouse cortical neurons, and this effect was completely lacking in ASIC1a KO neurons (Fig. 9*A*). Second, we performed Western blot to illustrate that the acidic solution treatment induced a significant increase in the phosphorylation of PKCλ in the cultured cortical neurons; however, this increase was blocked by the removal of Ca^{2+} from the treatment solution ($F_{(5,18)} = 1.27$, $p = 0.0448$, one-way ANOVA; Tukey's multiple-comparison test: WT-pH 7.4 vs WT-pH 6.0, $p = 0.0040$; WT-pH 7.4 vs WT-pH 6.0, Ca^{2+} free, $p = 0.8800$; Fig. 9*B*,*C*) or the incubation with BAPTA-AM to prevent the elevation of the intracellular Ca^{2+} ($F_{(5,18)} = 2.94$, $p = 0.0410$, one-way ANOVA; Tukey's multiple-comparison test: WT-pH 7.4 vs WT-pH 6.0, $p = 0.0072$; WT-pH 7.4 vs WT-pH 6.0, BAPTA-AM, $p = 0.9459$; Fig. 9*D*,*E*). Moreover, the acid-induced increase in PKCλ phosphorylation was not seen in ASIC1a KO neurons (Fig. 9*B*–*E*). These findings suggest that, in cortical neurons, acid activation of ASIC1a triggers PKCλ phosphorylation in a Ca^{2+}-dependent manner.

Blocking ASIC1a in ACC reverses established pain hypersensitivity

Finally, to address the possibility of targeting ASIC1a for pain management, we evaluated whether inhibiting ASIC1a could block the preestablished pain hypersensitivity. Interestingly, a post-treatment with intra-ACC administration of PcTx1 3 d after CFA administration reversed the established inflammatory pain hypersensitivity (Fig. 10*A*,*B*). The analgesic effect of PcTx1 on thermal hypersensitivity was clearly evident at 10 min after the drug administration and subsided at ~90 min ($F_{(1,9)} = 10.44$, $p = 0.0103$, two-way repeated-measures ANOVA; Tukey's multiple-comparison test: saline vs PcTx1, $p = 0.0002$, $p = 0.0034$, and $p = 0.1328$ for 10, 30, and 90 min, respectively; Fig. 10*B*). Considering the better drugability of small molecules, we further evaluated the synthetic ASIC1a inhibitor, compound 5b, through bilateral injection into ACC (100 μM, 0.5 μl per side) (Fig. 10*C*). Notably, the post-treatment with 5b attenuated thermal hypersensitivity in WT mice similarly as PcTx1 ($F_{(3,18)} = 27.94$, $p < 0.0001$, two-way repeated-measures ANOVA; Tukey's multiple-comparison test: saline vs 5b, $p = 0.0022$, $p = 0.0097$, $p = 0.0475$, and $p = 0.7320$ for 10 min, 30 min, 90 min, and 1 d, respectively; Fig. 10*D*) but did not further attenuate the already reduced thermal hypersensitivity in ASIC1a KO mice (two-way repeated-measures ANOVA followed by Tukey's multiple-comparison test: saline vs 5b, $p = 0.6219$, $p = 0.7168$, $p = 0.8536$, and $p = 0.7082$ for 10 min, 30 min, 90 min, and 1 d, respectively; Fig. 10*D*), confirming the specific involvement of ASIC1a in the drug effect.

Next, we tested whether ASIC1a antagonism has similar antihyperalgesic effects in other animal models of chronic pain. We used the well-established SNI model of neuropathic pain in adult mice as previously described (Bourquin et al., 2006; Tan et al., 2017). Post-treatment with intra-ACC administration of PcTx1 at 7 d after SNI significantly reversed the mechanical allodynia, with the analgesic effect lasting for at least 90 min ($F_{(1,9)} = 26.94$, $p = 0.0006$, two-way repeated-measures ANOVA; Tukey's multiple-comparison test: saline vs PcTx1, $p = 0.0004$, $p < 0.0001$, and $p = 0.0074$ for 10, 30, and 90 min, respectively; Fig. 10*E*,*F*). Similarly, bilateral injection of compound 5b also annulled the established mechanical hypersensitivity in the SNI model of neuropathic pain ($F_{(1,9)} = 9.08$, $p = 0.0146$, two-way repeated-measures ANOVA; Tukey's multiple-comparison test: saline vs 5b, $p = 0.0017$, $p = 0.0005$, $p < 0.0001$, and $p = 0.0055$ for 10 min, 30 min, 90 min, and 3 h, respectively; Fig. 10*G*,*H*). To rule out inflammation as a confounding contributor to hypersensitivity in the SNI model, we also tested the ASIC1a inhibitors at 14 d after SNI when the inflammatory response to surgery subsided. Again, the nerve injury-induced mechanical allodynia was

←

(*Figure legend continued.*) mechanical allodynia (***F***). $n = 8$ mice per group. ***G***, ***H***, Overexpression of PKCλ restored cingulate LTP induction ($n = 6$ slices/4 mice). ***G***, Summary plot of fEPSP slopes. Insets, Representative fEPSP traces at the time points indicated. Calibration: 100 μV, 10 ms. Arrow indicates the TBS application. ***H***, Induction ratios of cingulate LTP. ***I***, ***J***, Representative images (***I***) and quantification (***J***) of Western blots showing that PKCλ overexpression rescued CFA-induced membrane delivery of GluA1 in ACC of ASIC1a KO mice ($n = 4$ mice per group). ***K***, Schematic of the experimental procedure for PKCλ knockdown in conditional ASIC1a KO mice. ***L***, Schematic diagram of the viral vectors for AAV-hSyn-Ctrl, AAV-hSyn-Cre, AAV-NC-Ctrl, and AAV-PKCλ-shRNA. NC, Negative control. ***M***, ***N***, Representative images (***M***) and quantification (***N***) of Western blots demonstrating that AAV-PKCλ-shRNA injection significantly reduced expression of total and p-PKCλ in ACC of conditional ASIC1a KO mice ($n = 4$ mice per group). ***O***, ***P***, Genetic knockdown of PKCλ in ACC produced no further analgesic effects in either thermal (***O***) or mechanical (***P***) pain tests in the conditional ASIC1a KO mice (AAV-hSyn-Ctrl + AAV-NC-Ctrl, $n = 11$ mice; AAV-hSyn-Cre + AAV-NC-Ctrl, $n = 10$ mice; AAV-hSyn-Cre + AAV-PKCλ-shRNA, $n = 9$ mice). Data are mean ± SEM. *$p < 0.05$, **$p < 0.01$, ***$p < 0.001$, N.S., not significant.

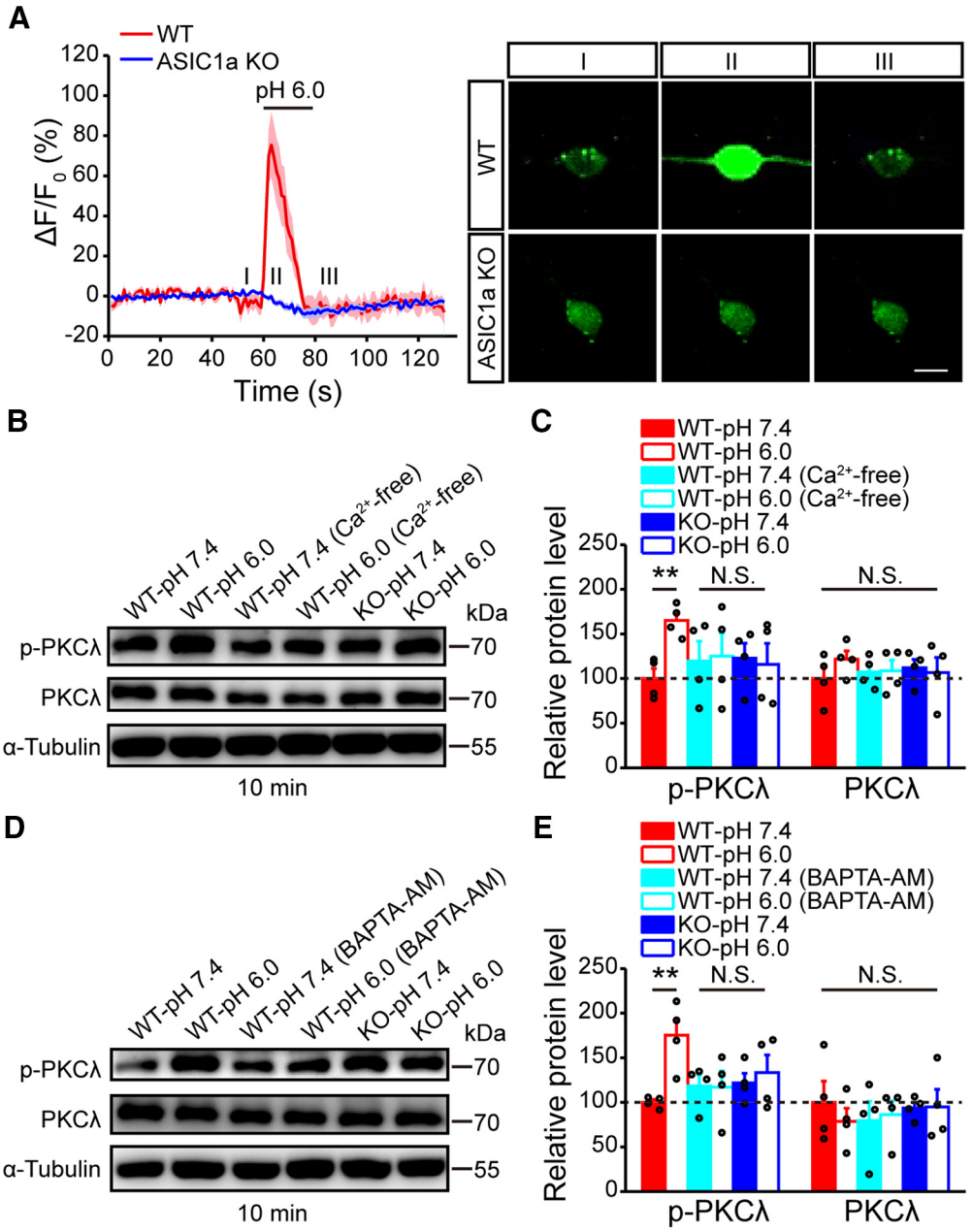

Figure 9. ASIC1a induces PKCλ phosphorylation through intracellular Ca^{2+} increase. ***A***, Acid (pH 6.0)-induced changes in cytosolic Ca^{2+} signal, indicated by GCaMP6 fluorescence, in cultured WT or ASIC1a KO mouse cortical neurons. $n = 9$ or 10. Thick lines indicate mean. Shaded areas represent SEM. Right, Representative images of GCaMP6-labeled neurons at indicated time points (I, II, and III). Scale bar, 10 μm. ***B***, ***C***, Representative images (***B***) and quantification (***C***) of Western blots showing that the acidic solution, pH 6.0, treatment elicited a significant increase in the phosphorylation of PKCλ in cultured cortical neurons from WT but not ASIC1a KO mice. A Ca^{2+}-free pH 6.0 solution failed to evoke PKCλ phosphorylation. $n = 4$. ***D***, ***E***, Representative images (***D***) and quantification (***E***) of Western blots showing that chelating intracellular Ca^{2+} by BAPTA-AM also eliminated the acidic solution-induced PKC phosphorylation. $n = 4$. $^{**}p < 0.01$, N.S., not significant.

attenuated by the intra-ACC administration of PcTx1 ($F_{(1,9)} = 6.90$, $p = 0.0275$, two-way repeated-measures ANOVA; Tukey's multiple-comparison test: saline vs PcTx1, $p = 0.0026$, $p = 0.0068$, and $p = 0.0464$ for 10, 30, and 90 min, respectively; Fig. 10*I*,*J*) and compound 5b ($F_{(1,9)} = 15.22$, $p = 0.0036$, two-way repeated-measures ANOVA; Tukey's multiple-comparison test: saline vs 5b, $p = 0.0001$, $p = 0.0004$, and $p = 0.0179$ for 10, 30, and 90 min, respectively; Fig. 10*K*,*L*). Together, these results suggest that cingulate ASIC1a can serve as a good target for future development of drugs against chronic pain, including both inflammatory and neuropathic types.

It has been suggested that ACC mainly plays a role in the affective (or aversive) component of pain. Several research groups, using multiple pain conditions and interventions, have shown that ACC excitation correlates with increased aversive responses to pain (LaGraize et al., 2004; LaGraize and Fuchs, 2007; Qu et al., 2011; Navratilova et al., 2015; Sellmeijer et al., 2018). Therefore, we tested whether ASIC1a in the ACC contributes to pain-related negative affect. We used pain-evoked PEAP to evaluate the affective responses to chronic pain as previously described (LaBuda and Fuchs, 2000; Han et al., 2014). Surprisingly, we found that postinjection of compound 5b, at the same dose as

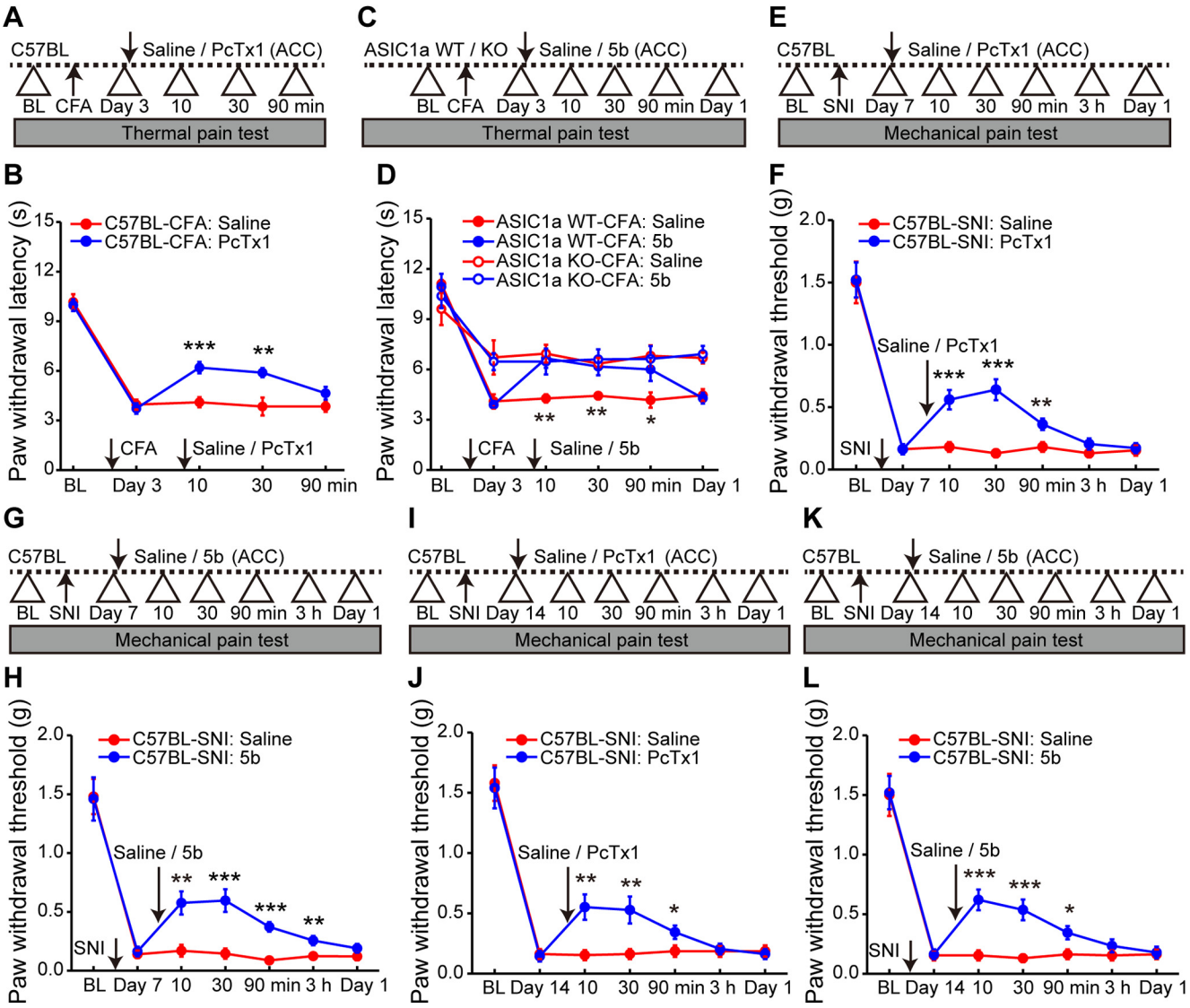

Figure 10. Inhibiting ASIC1a in ACC reverses the preestablished inflammatory and neuropathic pain hypersensitivity. ***A***, Schematic diagram of the experimental protocol for ***B***. PcTx1 was microinfused into ACC at day 3 after CFA injection. ***B***, Post-treatment with PcTx1 at ACC reversed CFA-induced thermal hyperalgesia. $n = 10$ mice for each group. ***C***, Schematic diagram of the experimental protocol for ***D***. Similar to ***A***, but another ASIC1a inhibitor, compound 5b, was injected in ACC to determine the analgesic effects. ***D***, Compound 5b significantly reversed inflammatory pain in WT mice but had no effect on ASIC1a KO mice, excluding any nonspecific action of compound 5b. $n = 10$ mice for each group. ***E***, Schematic diagram of the experimental protocol for ***F***. PcTx1 or saline was microinfused into ACC at day 7 after SNI. ***F***, Post-treatment with PcTx1 reversed SNI-induced mechanical allodynia. $n = 10$ mice for each group. ***G***, ***H***, Compound 5b produced a similar antihyperalgesia effect in the SNI model of neuropathic pain. $n = 10$ mice for each group. ***I***, Schematic diagram of the experimental protocol for ***J***. PcTx1 or saline was microinfused into ACC at day 14 after SNI. ***J***, Post-treatment with PcTx1 still reversed SNI-induced mechanical allodynia at the later stage of neuropathic pain. $n = 10$ mice for each group. ***K***, ***L***, Intra-ACC administration of compound 5b produced a similar antihyperalgesia effect at day 14 after SNI. $n = 10$ mice for each group. Data are mean ± SEM. $^*p < 0.05$, $^{**}p < 0.01$, $^{***}p < 0.001$.

that to produce the aforementioned antiallodynic effects, could not relieve the aversiveness of either CFA-induced inflammatory pain or SNI-induced neuropathic pain (Fig. 11). Compared with the control group (intraplantar saline plus intra-ACC saline, or sham injury plus intra-ACC saline), animals with intra-ACC administration of either saline or 5b spent significantly more time in the light half of the chamber to avoid stimulation of the inflamed hindpaw ($F_{(2,18)} = 268.3$, $p < 0.0001$, two-way repeated-measures ANOVA; Tukey's multiple-comparison test: CFA-saline vs CFA-5b, $p = 0.3155$, $p = 0.1334$, $p = 0.6613$, $p = 0.9904$, $p = 0.8928$, and $p = 0.7176$ for 5, 10, 15, 20, 25, and 30 min, respectively; Fig. 11*A*,*B*) or nerve-injured hindpaw (7 d after SNI: $F_{(2,18)} = 138.2$, $p < 0.0001$, two-way repeated-measures ANOVA; Tukey's multiple-comparison test: SNI-saline vs SNI-5b, $p = 0.9616$, $p = 0.9756$, $p = 0.5214$, $p = 0.1041$, $p = 0.4873$, and $p = 0.9861$ for 5, 10, 15, 20, 25, and 30 min, respectively; Fig. 11*C*,*D*; 14 d after SNI: $F_{(2,18)} = 154.5$, $p < 0.0001$, two-way repeated-measures ANOVA; Tukey's multiple-comparison test: SNI-saline vs SNI-5b, $p = 0.5072$, $p = 0.9133$, $p = 0.3663$, $p = 0.8990$, $p = 0.7721$, and $p = 0.4000$ for 5, 10, 15, 20, 25, and 30 min, respectively; Fig. 11*E*,*F*). These findings indicate that ASIC1a in the ACC contributes pain hypersensitivity through sensory, rather than affective, aspect of pain processing.

Discussion

ASIC1a channel has been well documented to contribute to pathophysiology of several neurological diseases, such as chronic pain (Duan et al., 2012), stroke (Wang et al., 2015), and epilepsy (Ziemann et al., 2008). The present study reveals a novel function of ASIC1a in ACC, where it is abundantly expressed and criti-

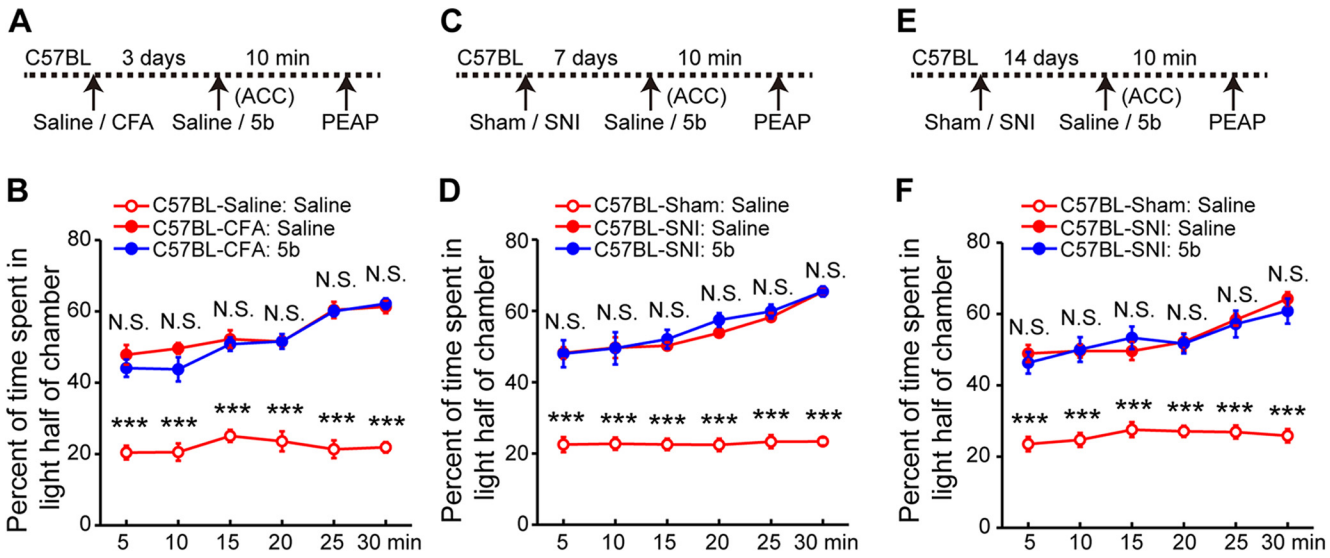

Figure 11. Inhibiting cingulate ASIC1a fails to affect chronic pain-related negative aversion. ***A***, Schematic diagram of the experimental protocol for ***B***. The PEAP test was performed at 10 min after 5b infusion at day 3 after CFA injection. ***B***, Intra-ACC administration of 5b did not reverse inflammatory pain-induced negative aversion in the PEAP. Compared with the saline-injected control group, CFA-inflamed animals with intra-ACC injection of either saline or 5b spent similarly more time in the light side of the chamber to avoid the noxious stimulation in the dark side. $n = 10$ mice for each group. ***C***, Schematic diagram of the experimental protocol for ***D***. The PEAP test was performed at 10 min after 5b infusion at day 7 after SNI induction. ***D***, Intra-ACC administration of 5b did not reverse neuropathic pain-induced negative aversion in the PEAP test. $n = 10$ mice for each group. ***E***, Schematic diagram of the experimental protocol for ***F***. The PEAP test was performed at 10 min after 5b infusion on day 14 after SNI induction. ***F***, Intra-ACC administration of 5b did not reverse SNI-induced negative aversion at the later stage of neuropathic pain. $n = 10$ mice for each group. $^{***}p < 0.001$, N.S., not significant.

cally involved in nociceptive hypersensitivity through modulating the strength of excitatory synaptic transmission. Specifically, we show that disrupting ASIC1a expression/or function in ACC by either genetic deletion or pharmacological blockade significantly relieves CFA-induced heat hyperalgesia and mechanical allodynia, as well as the enhancement of cortical synaptic adaptations caused by chronic inflammatory pain. Moreover, we reveal that ASIC1a participates in cingulate LTP induction through a PKCλ-dependent increase in GluA1 receptor membrane trafficking, eventually leading to enhanced synaptic efficacy and behavioral sensitization. This represents the first demonstration of the synaptic role of ASIC1a in ACC. Another novelty of this study lies in the demonstration of PKCλ in cortical processing of pain, while most previous studies have focused on the role of spinal PKCλ in nociceptive processing. More importantly, we show that the preestablished pain hypersensitivity can be reversed by drug inhibition of cingulate ASIC1a. These results not only extend our understanding of the supraspinal role of ASIC1a but also provide proof of principle for the therapeutic potential of targeting ASIC1a to treat chronic pain.

ASICs are excitatory cation channels directly gated by extracellular protons (Kellenberger and Schild, 2015). Growing studies have reported the importance of ASIC1a in multiple aspects of nociception as well as several animal models of chronic pain. However, the majority of these studies focused on the peripheral and spinal ASIC1a, with little attention paid to the function of cortical ASIC1a in pain processing (Wemmie et al., 2013; Deval and Lingueglia, 2015). Here, we demonstrate the role of ASIC1a in ACC by first showing its contribution to the development of inflammatory pain hypersensitivity. To selectively manipulate ASIC1a in ACC, we used a number of genetic and pharmacological strategies. First, we injected AAV-Cre virus into ACC of ASIC1a$^{flox/flox}$ mice to specifically delete the channel in this brain area. This resulted in attenuated heat and mechanical hypersensitivity in the CFA model of inflammatory pain. Second, we knocked down ASIC1a expression in ACC by shRNA and obtained similar analgesic effects. Third, preemptive treatment with PcTx1 reduced the elevated inflammatory pain sensitivity. Last, we selectively disrupted ASIC1a in excitatory neurons of ACC and showed them to be critical for inflammatory sensitization. Together, these findings strongly argue for the importance of cingulate ASIC1a in gating sensory hypersensitivity under inflammatory conditions.

It is well documented that ASIC1a, apart from being involved in multiple pathological processes, exerts its physiological functions by regulating synaptic transmission and plasticity in the brain (Huang et al., 2015). However, ASIC1a appears to play differential roles in synaptic plasticity in different brain regions. For instance, ASIC1a is important for LTP induction in hippocampus and amygdala (Du et al., 2014; Chiang et al., 2015; Liu et al., 2016), but it mainly regulates LTD inducibility in insular cortex (Li et al., 2016). These differences may underlie the variable effects of the channel on behavioral responses of various tasks. Here, we found ASIC1a to selectively regulate LTP induction in ACC. The exact reason(s) for the differential effects of ASIC1a on synaptic plasticity is not fully understood. The different locations of ASIC1a in distinct cell types from different brain regions, as well as the selective alterations in specific signaling pathways related to LTP or LTD resulting from ASIC1a inhibition, could all contribute to the diverse outcomes (Li et al., 2016). More interestingly, ASIC1a appears to use different downstream signaling pathways to regulate the same type of synaptic plasticity, such as LTP. In hippocampus, ASIC1a modulates LTP through both NMDAR-dependent and -independent pathways (Liu et al., 2016). In ACC, however, ASIC1a works through PKCλ to facilitate GluA1 synaptic delivery and in turn synaptic potentiation (see below). Therefore, the mechanisms by which ASIC1a regulates synaptic plasticity can be quite complex and diverse,

varying greatly depending on brain regions, cell types, and downstream signaling pathways.

LTP in sensory pathways has been proposed to be one of the most important cellular substrates for pain chronicity (Luo et al., 2014). The present results clearly show that ASIC1a is involved in both cingulate LTP and inflammatory pain hypersensitivity. To define the underlying mechanism, we focused on molecular processes that have been reported to contribute to LTP. A large body of literature supports the importance of AMPAR trafficking in LTP expression in several brain regions, including hippocampus and ACC (Toyoda et al., 2007; Penn et al., 2017; Zhou et al., 2018). Accordingly, we reveal that ASIC1a contributes to CFA-induced upregulation of membrane content of GluA1-containing AMPARs in ACC. This finding is in line with the previous report showing that ASIC1a promotes calcium-permeable AMPAR activity under conditions of ischemia or acidosis (Quintana et al., 2015). Interestingly, previous studies have stressed the NMDAR dependence of multiple ASIC1a-regulated functions, which occurs indirectly through ASIC1a-induced membrane depolarization due to Na^+ influx mediated by the channel (Gao et al., 2005; Wemmie et al., 2013; Yu et al., 2018). Although we do not exclude the possibility that ASIC1a contributes to cingulate LTP also through an NMDAR-dependent mechanism, our previous work indicates that ASIC1a mediates hippocampal LTP induction through both NMDAR-dependent and NMDAR-independent mechanisms. Thus, it would be important for future studies to determine whether and to what extent ASIC1a exerts its effect on cingulate LTP induction through NMDARs. The evidence collected here supports PKCλ as a critical mediator that links ASIC1a to GluA1 trafficking. Whereas the knockdown of PKCλ in ACC resulted in LTP impairment and behavioral analgesia, overexpression of exogenous PKCλ in ACC restored inflammatory hyperalgesia in ASIC1a KO mice. More critically, the knockdown of PKCλ did not further increase the pain threshold in conditional ASIC1a KO mice, making it unlikely that ASIC1a and PKCλ play parallel or additive roles in cingulate LTP and inflammatory pain. Our findings strongly suggest that ASIC1a promotes cingulate LTP and pain sensitization through, at least partially, PKCλ-regulated membrane trafficking of GluA1. In line with this assessment, previous work has shown PKCλ to be crucial for synaptic incorporation of AMPARs during hippocampal LTP and trace fear conditioning (Ren et al., 2013; Wang et al., 2016). Together, our present study adds a new dimension for cortical function of PKCλ, revealing its regulation by ASIC1a and contribution to cortical synaptic potentiation and behavioral sensitization to inflammatory pain.

Modulation of ion channel signaling has the potential to effectively treat pain. Ion channel modulators, such as lidocaine and pregabalin, act on voltage-gated sodium channels and calcium channels to reduce pain in the clinical setting (Skerratt and West, 2015). As a type of nonclassical ion channels, ASIC1a plays an important role in chronic pain processing at both peripheral and central levels of the sensory axis (Deval and Lingueglia, 2015). Moreover, deletion or inhibition of ASIC1a does not obviously affect normal sensation or other important physiological functions, which may make ASIC1a a better druggable target with fewer adverse effects. The present results clearly show that not only can a peptide inhibitor of ASIC1a, PcTx1, reverse the established pain hypersensitivity with intra-ACC administration, but the novel small-molecule inhibitor of ASIC1a, compound 5b, also exerts a similar analgesic effect. Importantly, the analgesic effect was demonstrated in both inflammatory and neuropathic pain models. Because of great difficulties in delivering large peptides for clinical use, the small-molecule-based 5b provides an excellent base for developing more potent and orally available ASIC1a drugs to alleviate chronic pain in the future.

In conclusion, we report the supraspinal role of cortically located ASIC1a in pain processing using multiple neurobiological approaches. ASIC1a critically gates pain sensitivity through regulating the probability of cingulate LTP induction, in which PKCλ serves as a crucial mediator. Together with previous reports on the pronociceptive function of ASIC1a in peripheral and spinal levels, our findings highlight the promising potential of targeting ASIC1a for future development of new molecular medications for chronic pain. This is of great clinical significance considering the huge unmet need in clinical pain management.

References

Berta T, Park CK, Xu ZZ, Xie RG, Liu T, Lü N, Liu YC, Ji RR (2014) Extracellular caspase-6 drives murine inflammatory pain via microglial TNF-alpha secretion. J Clin Invest 124:1173–1186.

Bliss TV, Collingridge GL, Kaang BK, Zhuo M (2016) Synaptic plasticity in the anterior cingulate cortex in acute and chronic pain. Nat Rev Neurosci 17:485–496.

Bohlen CJ, Chesler AT, Sharif-Naeini R, Medzihradszky KF, Zhou S, King D, Sánchez EE, Burlingame AL, Basbaum AI, Julius D (2011) A heteromeric Texas coral snake toxin targets acid-sensing ion channels to produce pain. Nature 479:410–414.

Bourquin AF, Suveges M, Pertin M, Gilliard N, Sardy S, Davison AC, Spahn DR, Decosterd I (2006) Assessment and analysis of mechanical allodynia-like behavior induced by spared nerve injury (SNI) in the mouse. Pain 122:14.e1–14.e14.

Buta A, Maximyuk O, Kovalskyy D, Sukach V, Vovk M, Ievglevskyi O, Isaeva E, Isaev D, Savotchenko A, Krishtal O (2015) Novel potent orthosteric antagonist of ASIC1a prevents NMDAR-dependent LTP induction. J Med Chem 58:4449–4461.

Chaplan SR, Bach FW, Pogrel JW, Chung JM, Yaksh TL (1994) Quantitative assessment of tactile allodynia in the rat paw. J Neurosci Methods 53:55–63.

Chen G, Park CK, Xie RG, Ji RR (2015) Intrathecal bone marrow stromal cells inhibit neuropathic pain via TGF-beta secretion. J Clin Invest 125:3226–3240.

Chen LM (2018) Cortical representation of pain and touch: evidence from combined functional neuroimaging and electrophysiology in non-human primates. Neurosci Bull 34:165–177.

Chen T, Taniguchi W, Chen QY, Tozaki-Saitoh H, Song Q, Liu RH, Koga K, Matsuda T, Kaito-Sugimura Y, Wang J, Li ZH, Lu YC, Inoue K, Tsuda M, Li YQ, Nakatsuka T, Zhuo M (2018) Top-down descending facilitation of spinal sensory excitatory transmission from the anterior cingulate cortex. Nat Commun 9:1886.

Chiang PH, Chien TC, Chen CC, Yanagawa Y, Lien CC (2015) ASIC-dependent LTP at multiple glutamatergic synapses in amygdala network is required for fear memory. Sci Rep 5:10143.

Chizh BA, Headley PM, Tzschentke TM (2001) NMDA receptor antagonists as analgesics: focus on the NR2B subtype. Trends Pharmacol Sci 22:636–642.

Deval E, Lingueglia E (2015) Acid-sensing ion channels and nociception in the peripheral and central nervous systems. Neuropharmacology 94:49–57.

Diochot S, Baron A, Salinas M, Douguet D, Scarzello S, Dabert-Gay AS, Debayle D, Friend V, Alloui A, Lazdunski M, Lingueglia E (2012) Black mamba venom peptides target acid-sensing ion channels to abolish pain. Nature 490:552–555.

Du J, Reznikov LR, Price MP, Zha XM, Lu Y, Moninger TO, Wemmie JA, Welsh MJ (2014) Protons are a neurotransmitter that regulates synaptic plasticity in the lateral amygdala. Proc Natl Acad Sci U S A 111:8961–8966.

Duan B, Liu DS, Huang Y, Zeng WZ, Wang X, Yu H, Zhu MX, Chen ZY, Xu TL (2012) PI3-kinase/Akt pathway-regulated membrane insertion of acid-sensing ion channel 1a underlies BDNF-induced pain hypersensitivity. J Neurosci 32:6351–6363.

Escoubas P, De Weille JR, Lecoq A, Diochot S, Waldmann R, Champigny G, Moinier D, Ménez A, Lazdunski M (2000) Isolation of a tarantula toxin

specific for a class of proton-gated Na^+ channels. J Biol Chem 275:25116–25121.

Ettinger AB, LoPresti A, Yang H, Williams B, Zhou S, Fain R, Laurenza A (2015) Psychiatric and behavioral adverse events in randomized clinical studies of the noncompetitive AMPA receptor antagonist perampanel. Epilepsia 56:1252–1263.

Gao J, Duan B, Wang DG, Deng XH, Zhang GY, Xu L, Xu TL (2005) Coupling between NMDA receptor and acid-sensing ion channel contributes to ischemic neuronal death. Neuron 48:635–646.

Han M, Xiao X, Yang Y, Huang RY, Cao H, Zhao ZQ, Zhang YQ (2014) SIP30 is required for neuropathic pain-evoked aversion in rats. J Neurosci 34:346–355.

Holmes D (2016) The pain drain. Nature 535:S2–S3.

Huang Y, Jiang N, Li J, Ji YH, Xiong ZG, Zha XM (2015) Two aspects of ASIC function: synaptic plasticity and neuronal injury. Neuropharmacology 94:42–48.

Huganir RL, Nicoll RA (2013) AMPARs and synaptic plasticity: the last 25 years. Neuron 80:704–717.

Kang SJ, Kwak C, Lee J, Sim SE, Shim J, Choi T, Collingridge GL, Zhuo M, Kaang BK (2015) Bidirectional modulation of hyperalgesia via the specific control of excitatory and inhibitory neuronal activity in the ACC. Mol Brain 8:81.

Kellenberger S, Schild L (2015) International Union of Basic and Clinical Pharmacology: XCI. Structure, function, and pharmacology of acid-sensing ion channels and the epithelial Na^+ channel. Pharmacol Rev 67:1–35.

Ko HG, Choi JH, Park DI, Kang SJ, Lim CS, Sim SE, Shim J, Kim JI, Kim S, Choi TH, Ye S, Lee J, Park P, Kim S, Do J, Park J, Islam MA, Kim HJ, Turck CW, Collingridge GL, et al. (2018) Rapid turnover of cortical NCAM1 regulates synaptic reorganization after peripheral nerve injury. Cell Rep 22:748–759.

Koga K, Descalzi G, Chen T, Ko HG, Lu J, Li S, Son J, Kim T, Kwak C, Huganir RL, Zhao MG, Kaang BK, Collingridge GL, Zhuo M (2015) Coexistence of two forms of LTP in ACC provides a synaptic mechanism for the interactions between anxiety and chronic pain. Neuron 85:377–389.

Kreple CJ, Lu Y, Taugher RJ, Schwager-Gutman AL, Du J, Stump M, Wang Y, Ghobbeh A, Fan R, Cosme CV, Sowers LP, Welsh MJ, Radley JJ, LaLumiere RT, Wemmie JA (2014) Acid-sensing ion channels contribute to synaptic transmission and inhibit cocaine-evoked plasticity. Nat Neurosci 17:1083–1091.

Kutsuwada T, Sakimura K, Manabe T, Takayama C, Katakura N, Kushiya E, Natsume R, Watanabe M, Inoue Y, Yagi T, Aizawa S, Arakawa M, Takahashi T, Nakamura Y, Mori H, Mishina M (1996) Impairment of suckling response, trigeminal neuronal pattern formation, and hippocampal LTD in NMDA receptor epsilon 2 subunit mutant mice. Neuron 16:333–344.

LaBuda CJ, Fuchs PN (2000) A behavioral test paradigm to measure the aversive quality of inflammatory and neuropathic pain in rats. Exp Neurol 163:490–494.

LaGraize SC, Fuchs PN (2007) GABAA but not GABAB receptors in the rostral anterior cingulate cortex selectively modulate pain-induced escape/avoidance behavior. Exp Neurol 204:182–194.

LaGraize SC, Labuda CJ, Rutledge MA, Jackson RL, Fuchs PN (2004) Differential effect of anterior cingulate cortex lesion on mechanical hypersensitivity and escape/avoidance behavior in an animal model of neuropathic pain. Exp Neurol 188:139–148.

Latremoliere A, Costigan M (2018) Combining human and rodent genetics to identify new analgesics. Neurosci Bull 34:143–155.

Li WG, Liu MG, Deng S, Liu YM, Shang L, Ding J, Hsu TT, Jiang Q, Li Y, Li F, Zhu MX, Xu TL (2016) ASIC1a regulates insular long-term depression and is required for the extinction of conditioned taste aversion. Nat Commun 7:13770.

Li XY, Ko HG, Chen T, Descalzi G, Koga K, Wang H, Kim SS, Shang Y, Kwak C, Park SW, Shim J, Lee K, Collingridge GL, Kaang BK, Zhuo M (2010) Alleviating neuropathic pain hypersensitivity by inhibiting PKMzeta in the anterior cingulate cortex. Science 330:1400–1404.

Liu MG, Zhuo M (2014) No requirement of TRPV1 in long-term potentiation or long-term depression in the anterior cingulate cortex. Mol Brain 7:27.

Liu MG, Li HS, Li WG, Wu YJ, Deng SN, Huang C, Maximyuk O, Sukach V, Krishtal O, Zhu MX, Xu TL (2016) Acid-sensing ion channel 1a contributes to hippocampal LTP inducibility through multiple mechanisms. Sci Rep 6:23350.

Luo C, Kuner T, Kuner R (2014) Synaptic plasticity in pathological pain. Trends Neurosci 37:343–355.

Marchand F, D'Mello R, Yip PK, Calvo M, Muller E, Pezet S, Dickenson AH, McMahon SB (2011) Specific involvement of atypical PKCzeta/PKMzeta in spinal persistent nociceptive processing following peripheral inflammation in rat. Mol Pain 7:86.

Mazzuca M, Heurteaux C, Alloui A, Diochot S, Baron A, Voilley N, Blondeau N, Escoubas P, Gélot A, Cupo A, Zimmer A, Zimmer AM, Eschalier A, Lazdunski M (2007) A tarantula peptide against pain via ASIC1a channels and opioid mechanisms. Nat Neurosci 10:943–945.

Navratilova E, Xie JY, Meske D, Qu C, Morimura K, Okun A, Arakawa N, Ossipov M, Fields HL, Porreca F (2015) Endogenous opioid activity in the anterior cingulate cortex is required for relief of pain. J Neurosci 35:7264–7271.

Paoletti P, Bellone C, Zhou Q (2013) NMDA receptor subunit diversity: impact on receptor properties, synaptic plasticity and disease. Nat Rev Neurosci 14:383–400.

Penn AC, Zhang CL, Georges F, Royer L, Breillat C, Hosy E, Petersen JD, Humeau Y, Choquet D (2017) Hippocampal LTP and contextual learning require surface diffusion of AMPA receptors. Nature 549:384–388.

Qu C, King T, Okun A, Lai J, Fields HL, Porreca F (2011) Lesion of the rostral anterior cingulate cortex eliminates the aversiveness of spontaneous neuropathic pain following partial or complete axotomy. Pain 152:1641–1648.

Quintana P, Soto D, Poirot O, Zonouzi M, Kellenberger S, Muller D, Chrast R, Cull-Candy SG (2015) Acid-sensing ion channel 1a drives AMPA receptor plasticity following ischaemia and acidosis in hippocampal CA1 neurons. J Physiol 593:4373–4386.

Ren SQ, Yan JZ, Zhang XY, Bu YF, Pan WW, Yao W, Tian T, Lu W (2013) PKCλ is critical in AMPA receptor phosphorylation and synaptic incorporation during LTP. EMBO J 32:1365–1380.

Roques BP, Fournié-Zaluski MC, Wurm M (2012) Inhibiting the breakdown of endogenous opioids and cannabinoids to alleviate pain. Nat Rev Drug Discov 11:292–310.

Sellmeijer J, Mathis V, Hugel S, Li XH, Song Q, Chen QY, Barthas F, Lutz PE, Karatas M, Luthi A, Veinante P, Aertsen A, Barrot M, Zhuo M, Yalcin I (2018) Hyperactivity of anterior cingulate cortex areas 24a/24b drives chronic pain-induced anxiodepressive-like consequences. J Neurosci 38:3102–3115.

Skerratt SE, West CW (2015) Ion channel therapeutics for pain. Channels 9:344–351.

Song Q, Zheng HW, Li XH, Huganir RL, Kuner T, Zhuo M, Chen T (2017) Selective phosphorylation of AMPA receptor contributes to the network of long-term potentiation in the anterior cingulate cortex. J Neurosci 37:8534–8548.

Suzuki A, Akimoto K, Ohno S (2003) Protein kinase C λ/ι (PKCλ/ι): a PKC isotype essential for the development of multicellular organisms. J Biochem 133:9–16.

Tan LL, Pelzer P, Heinl C, Tang W, Gangadharan V, Flor H, Sprengel R, Kuner T, Kuner R (2017) A pathway from midcingulate cortex to posterior insula gates nociceptive hypersensitivity. Nat Neurosci 20:1591–1601.

Toyoda H, Wu LJ, Zhao MG, Xu H, Zhuo M (2007) Time-dependent postsynaptic AMPA GluR1 receptor recruitment in the cingulate synaptic potentiation. Dev Neurobiol 67:498–509.

Volk LJ, Bachman JL, Johnson R, Yu Y, Huganir RL (2013) PKM-zeta is not required for hippocampal synaptic plasticity, learning and memory. Nature 493:420–423.

Wang H, Xu H, Wu LJ, Kim SS, Chen T, Koga K, Descalzi G, Gong B, Vadakkan KI, Zhang X, Kaang BK, Zhuo M (2011) Identification of an adenylyl cyclase inhibitor for treating neuropathic and inflammatory pain. Sci Transl Med 3:65ra63.

Wang Q, Wang Q, Song XL, Jiang Q, Wu YJ, Li Y, Yuan TF, Zhang S, Xu NJ, Zhu MX, Li WG, Xu TL (2018) Fear extinction requires ASIC1a-dependent regulation of hippocampal-prefrontal correlates. Sci Adv 4:eaau3075.

Wang S, Sheng T, Ren S, Tian T, Lu W (2016) Distinct roles of PKCiota/λ and PKMζ in the initiation and maintenance of hippocampal long-term potentiation and memory. Cell Rep 16:1954–1961.

Wang YZ, Wang JJ, Huang Y, Liu F, Zeng WZ, Li Y, Xiong ZG, Zhu MX, Xu

TL (2015) Tissue acidosis induces neuronal necroptosis via ASIC1a channel independent of its ionic conduction. eLife 4:e05682.
Waxman SG, Zamponi GW (2014) Regulating excitability of peripheral afferents: emerging ion channel targets. Nat Neurosci 17:153–163.
Wemmie JA, Chen J, Askwith CC, Hruska-Hageman AM, Price MP, Nolan BC, Yoder PG, Lamani E, Hoshi T, Freeman JH Jr, Welsh MJ (2002) The acid-activated ion channel ASIC contributes to synaptic plasticity, learning, and memory. Neuron 34:463–477.
Wemmie JA, Askwith CC, Lamani E, Cassell MD, Freeman JH Jr, Welsh MJ (2003) Acid-sensing ion channel 1 is localized in brain regions with high synaptic density and contributes to fear conditioning. J Neurosci 23:5496–5502.
Wemmie JA, Taugher RJ, Kreple CJ (2013) Acid-sensing ion channels in pain and disease. Nat Rev Neurosci 14:461–471.
Woolf CJ (2010) Overcoming obstacles to developing new analgesics. Nat Med 16:1241–1247.
Wu LJ, Zhuo M (2009) Targeting the NMDA receptor subunit NR2B for the treatment of neuropathic pain. Neurotherapeutics 6:693–702.
Wu LJ, Duan B, Mei YD, Gao J, Chen JG, Zhuo M, Xu L, Wu M, Xu TL (2004) Characterization of acid-sensing ion channels in dorsal horn neurons of rat spinal cord. J Biol Chem 279:43716–43724.
Wu PY, Huang YY, Chen CC, Hsu TT, Lin YC, Weng JY, Chien TC, Cheng IH, Lien CC (2013) Acid-sensing ion channel-1a is not required for normal hippocampal LTP and spatial memory. J Neurosci 33:1828–1832.
Xu H, Wu LJ, Wang H, Zhang X, Vadakkan KI, Kim SS, Steenland HW, Zhuo M (2008) Presynaptic and postsynaptic amplifications of neuropathic pain in the anterior cingulate cortex. J Neurosci 28:7445–7453.
Yekkirala AS, Roberson DP, Bean BP, Woolf CJ (2017) Breaking barriers to novel analgesic drug development. Nat Rev Drug Discov 16:545–564.
Yu Z, Wu YJ, Wang YZ, Liu DS, Song XL, Jiang Q, Li Y, Zhang S, Xu NJ, Zhu MX, Li WG, Xu TL (2018) The acid-sensing ion channel ASIC1a mediates striatal synapse remodeling and procedural motor learning. Sci Signal 11:eaar4481.
Zamanillo D, Sprengel R, Hvalby O, Jensen V, Burnashev N, Rozov A, Kaiser KM, Köster HJ, Borchardt T, Worley P, Lübke J, Frotscher M, Kelly PH, Sommer B, Andersen P, Seeburg PH, Sakmann B (1999) Importance of AMPA receptors for hippocampal synaptic plasticity but not for spatial learning. Science 284:1805–1811.
Zamponi GW (2016) Targeting voltage-gated calcium channels in neurological and psychiatric diseases. Nat Rev Drug Discov 15:19–34.
Zeng WZ, Liu DS, Duan B, Song XL, Wang X, Wei D, Jiang W, Zhu MX, Li Y, Xu TL (2013) Molecular mechanism of constitutive endocytosis of acid-sensing ion channel 1a and its protective function in acidosis-induced neuronal death. J Neurosci 33:7066–7078.
Zhao MG, Ko SW, Wu LJ, Toyoda H, Xu H, Quan J, Li J, Jia Y, Ren M, Xu ZC, Zhuo M (2006) Enhanced presynaptic neurotransmitter release in the anterior cingulate cortex of mice with chronic pain. J Neurosci 26:8923–8930.
Zhou Z, Liu A, Xia S, Leung C, Qi J, Meng Y, Xie W, Park P, Collingridge GL, Jia Z (2018) The C-terminal tails of endogenous GluA1 and GluA2 differentially contribute to hippocampal synaptic plasticity and learning. Nat Neurosci 21:50–62.
Ziemann AE, Schnizler MK, Albert GW, Severson MA, Howard MA 3rd, Welsh MJ, Wemmie JA (2008) Seizure termination by acidosis depends on ASIC1a. Nat Neurosci 11:816–822.